RSC Advances

Influence of Graphene Oxide as Dispersed Phase in Cement Mortar Matrix in Defining the Crystal Patterns of Cement Hydrates and its Effect on Mechanical, Microstructural and Crystallization Properties

Journal:	*RSC Advances*
Manuscript ID:	RA-ART-05-2015-008078
Article Type:	Paper
Date Submitted by the Author:	02-May-2015
Complete List of Authors:	Kothiyal, Navin; Dr. B R Ambedkar National Institute of Technology Jalandhar, Chemistry; Dr. B R Ambedkar National Institute of Technology Jalandhar, Chemistry Sharma, Snigdha; Dr. B R Ambedkar National Institute of Technology, Jalandhar, Department of Chemistry

Influence of Graphene Oxide as Dispersed Phase in Cement Mortar Matrix in Defining the Crystal Patterns of Cement Hydrates and its Effect on Mechanical, Microstructural and Crystallization Properties

Snigdha Sharma and N.C. Kothiyal*

Department of Chemistry, Dr B R Ambedkar National Institute of Technology, Jalandhar – 144011 (Punjab) India

E-mail: snigdha.sharma343@gmail.com; Tel.: +91-98889-22574

Corresponding Author: E- mail: kothiyalnc@nitj.ac.in; Tel.: +91-94172-74496

Abstract

In present investigation, Graphene Oxide (GO) was prepared using oxidative treatment of graphite by Hummer's Method. Synthesized graphene oxide (GO_a) was characterized by FTIR, SEM/EDS, TEM, XRD, TGA and AFM. Size-reduction of GO_a (14 nm sheet thickness and 900 nm average sheet size) was done using planetary ball milling, which produced GO_b with 3 nm sheet thickness and 100 nm average sheet size. Effectiveness of GO_a and GO_b nanosheets at different dosages (by wt% of cement) in improvement of mechanical strength of cement mortar matrix was evaluated and was explained on basis of microstructural analysis using FE-SEM observations as well as crystallization patterns using XRD patterns of GO-Cement Nanocomposites (GO-CNCs). Well- defined crystal growths of cement hydrates were observed as revealed by FE-SEM micrographs and crystal patterns were found to be dependent upon factors such as type of GO nanosheets, concentration of GO and curing time. As-synthesized GO_a (1% by wt. of cement) enhanced compressive strength of composites by maximum 63% whereas size-reduced GO_b (1% by wt. of cement) promoted better crystalline structures with the maximum strength enhancement of 86%. Present research work aims to enhance GO reactivity by increasing its exfoliation and its count by mechanical milling and to exploit it as a low-cost dispersed phase having different sheet thicknesses and sheet sizes for strength enhancement of cementitious matrix by regulating crystal patterns and microstructural features.

Corresponding Author, Tel.: +91-9417274496; Fax: +91-0181-2690320; E- mail: kothiyalnc@nitj.ac.in (N.C. Kothiyal)

Keywords: GO – Cement Nanocomposites (GO-CNCs); Crystal Patterns; Cement Hydrates; Microstructure, Compressive Strength, Ball Milling.

Graphical abstract

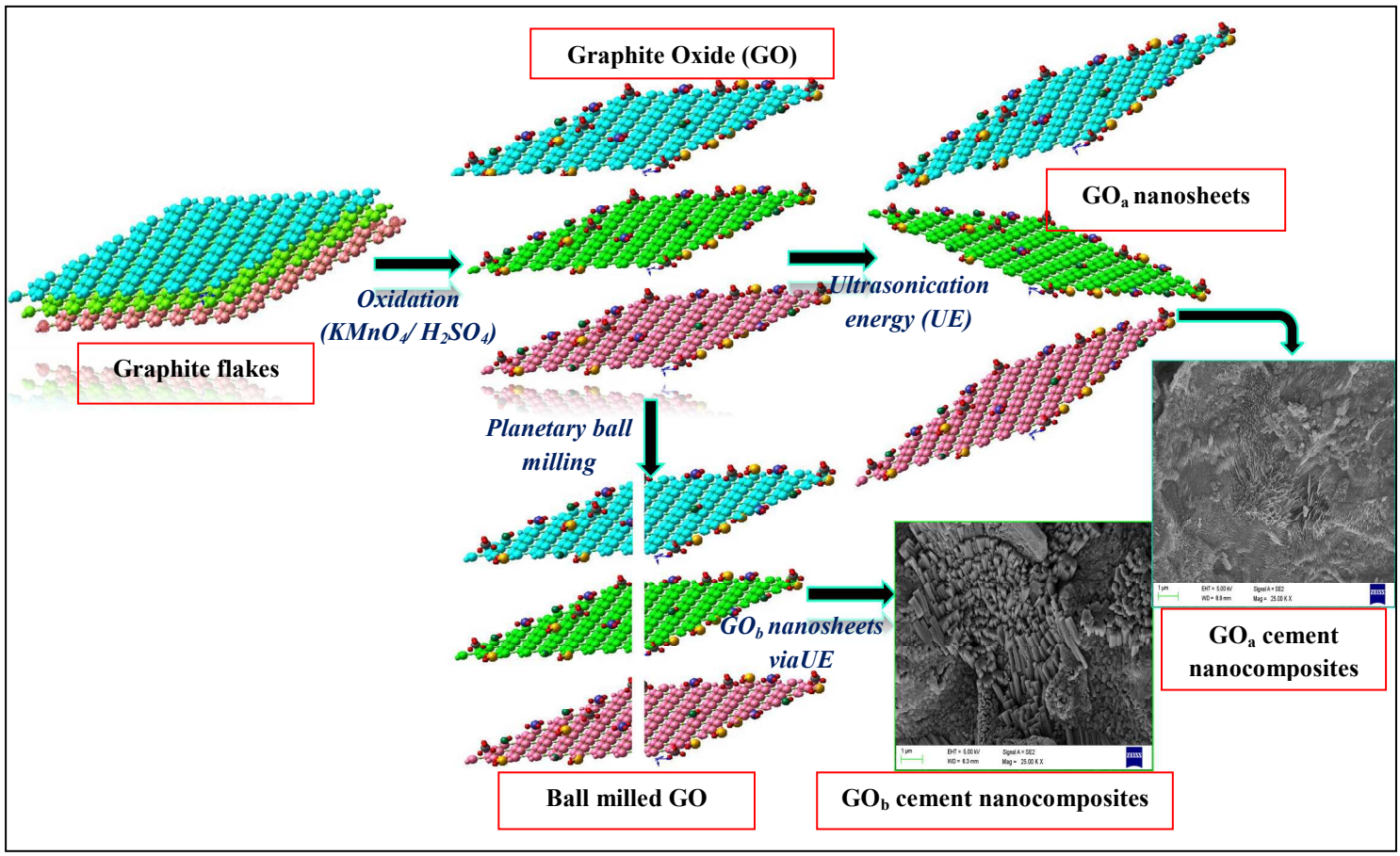

1. Introduction

Portland cement, mortar and concrete are the most commonly used construction materials worldwide. However, the inherent quasi – brittle behavior of cement makes the associated cracking rapid in these materials, thereby leading to the disintegration of cement – based materials. The deformation process of cementitious matrix involves the initiation, propagation and coalescence of microcracks.[1] These challenges have been resolved by the use of high – performance cementitious composites.[2] Various researchers have employed the incorporation of fibers with different shapes and geometries to arrest the cracking phenomenon, which mainly includes steel bars,[3] steel fibers,[4-6] glass fibers,[7,8] carbon fibers,[9] polypropylene fibers[10,11] and

various others.[12] These reinforcing materials exhibit their reinforcement either at macro - level or micro - level and therefore cannot arrest the cracks originating at nanoscale. This consequently affects the toughness and durability of cementitious matrix.

To overcome these drawbacks, investigations have been shifted to the use of nanofibers (i.e. CNFs or CNTs). CNFs and CNTs have been the materials of interest for past few years[13-15] and have shown remarkable improvements in mechanical properties of cement based materials on account of their crack – bridging effects at nanoscale[16] and nucleation effect for formation of different cement hydrates.[17,18]

These cement hydrates are the products of complex hydration reactions of major compounds (silicates and aluminates of calcium) present in the cement i.e. tricalcium silicate (C_3S, $3CaO{\cdot}SiO_2$), dicalcium silicate (C_2S, $2CaO{\cdot}SiO_2$), tricalcium aluminate (C_3A, $3CaO{\cdot}Al_2O_3$), tetracalcium aluminoferrite (C_4AF, $4CaO{\cdot}Al_2O_3{\cdot}Fe_2O_3$) and gypsum ($CaSO_4{\cdot}2H_2O$).[2] They produce complex products, such as calcium silicate hydrate (C–S–H), calcium hydroxide (CH), ettringite (AFt) and monosulfates (AFm). The final strength of cement based materials is dependent on the amount of these cement hydrates as well as their crystal shapes which may be platy, elongated, rod shaped, etc. Incorporation of CNFs and CNTs can boost up the quantity of these crystalline products but are incapable of controlling the growth pattern of crystals. Moreover, these nanomaterials are very costly for their practical applications and have major drawback of poor dispersion properties in most of the matrices.[19] Either they need chemical modification of their surface[20,21] or use of surfactants[22] which might influence the hydration reactions of cement compounds due to their incompatibility.

There is a need to regulate the microstructure of cementitious matrix using a material which is not only cost – effective for its practical application from industrial point of view but can also work at nanoscale apart from having better dispersibility in the matrix. Recent emergence of graphene oxide (GO) can act as possible solution to the same since the material has unique properties like very high surface area,[23] surface functionalization[24] and good dispersion in aqueous solvents.[25,26] The material has shown promising results when used as reinforcing material in different kinds of matrices.[27-30] A few researchers have investigated the influence of GO on the mechanical properties of cement based materials[31] using concentration levels of GO ranging from 0.01 % to 0.06% by wt. of cement and have achieved remarkable results. Till date,

no studies have been reported on the reinforcement effect of GO nanosheets beyond 0.1% concentration level in the cementitious matrix.

Planetary ball – milling is one of the techniques to obtain the nanopowders in their smallest possible particle size in bulk form and in relatively shorter milling times under carefully controlled conditions.[32,33] To increase the exfoliation and surface area of GO, ball – milling can prove to be an effective technique. This can be achieved by ball – milling either the starting precursor graphite used for its synthesis or the synthesized GO. Due to strong interplanar forces of attraction, exfoliation and size – reduction of stacked graphite takes very long milling times and is highly time consuming (usually greater than 50 hrs).[34] Agglomeration of fragmented particles of graphite is also one of the drawbacks since they lack any surface functionalization. Moreover, exfoliation of graphite requires costly dispersion mediums during ball milling process.[35] In contrast, weak vander waals forces between GO layers are helpful in making the exfoliation and size – reduction rapid as well as time – saving. This not only makes the GO nanosized but also reduces the sheet thickness by virtue of exfoliation.

A very limited research has been carried out on the incorporation of ball – milled GO nanosheets in the cement mortar matrix. Present investigation was therefore aimed to evaluate the effectiveness of two different types of GO nanosheets having different sizes on the mechanical strength of hardened cement mortar matrix, at concentration levels ranging from 0.125% to 1.00% by wt. of cement. The size and thickness of original GO nanosheets synthesized in our laboratory was further reduced to smallest possible size using one of the basic techniques of size – reduction i.e. planetary ball – milling. Both the original GO nanosheets as well as size- reduced GO nanosheets were compared for their effect on cement mortar at same concentration levels at increasing curing times of 7, 14 and 28 days. GO – cement nanocomposites fabricated were further investigated for their microstructure and the quantitative cement hydrates and crystalline products.

Present investigation provides a pathway to enhance the effectiveness and reactivity of GO nanosheets via exfoliation using ball – milling technique. The research provides a pathway to exploit GO as an economical dispersed phase in contribution to improve the mechanical peformance, microstructural features and crystalline behavior of cementitious materials.

2. Experimental Section

2.1. Materials and Chemicals

Graphite (particle size 100 μm) was purchased from local dealers. Analytical grade chemicals were used in the present investigation and were procured from Merck Specialty Pvt. Ltd. (India). The chemicals used were concentrated sulphuric acid (H_2SO_4, 98%), potassium permanganate ($KMnO_4$), sodium nitrate ($NaNO_3$) and hydrogen peroxide (H_2O_2, 30%).

Ordinary Portland cement (Grade 43) was procured from ACC Ltd. (India). The chemical properties of cement used in the study are shown in Table 1. Indian standard sand (Grade I, Grade II and Grade III) following IS 650:1991 with an average specific gravity of 2.64 was procured from Tamin, Ennore (India). Three grades of standard sand were used in equal proportions of 33.33% each. The specifications of sand used in study are shown in Table 2. Particle size distribution of fine aggregates is shown in Fig. 1, from which it can be observed that aggregates used in the study are well-graded. The fineness modulus of fine aggregates used is 2.496. Polycarboxylate superplasticizer (Glenium) was procured from BASF India Ltd. (India). Superplasticizer (PC) was used to achieve the required workability of cement mortar mixes and to improve dispersion of GO in cementitious matrix. The percentage of PC used was considered as ineffective on strength properties of the mixes.[31]

All the materials were used as received.

Table 1 Chemical Properties of OPC

Table 2 Specifications of Indian Standard Sand

Fig. 1 Sieve analysis of fine aggregates (equal proportion of Grade I, II and III) showing particle size distribution

2.2. Synthesis of GO sheets

Firstly, 5 g Graphite powder, 114 ml 98% H_2SO_4 and 2.5 g $NaNO_3$ were added sequentially to a round-bottom flask which was then placed in an ice bath (~5^0C) under continuous stirring on a magnetic stirrer. The contents of the flask were subjected to continuous stirring for about 15 – 20 minutes. 15 g $KMnO_4$ was added very slowly in small lots to the flask. The ice bath was now removed and the suspension temperature was maintained around 36^0C for ~30 minutes. On progressing the reaction, the mixture gradually thickened. Then 100 ml of deionized water was slowly added to the suspension following 25 ml H_2O_2 addition dropwise into it. The color of the

solution changed from brown to bright yellow. The bright yellow suspension so obtained was then filtered by vacuum suction and repeated washings with deionized water were given in order to make the filtered product free of SO_4^{2-} ions. The product was vacuum dried for 10 hours and marked as GO_a.

2.3. Structural characterization of synthesized GO_a

The starting synthesized material were then characterized using FT-IR spectroscopy to monitor the presence of functional groups, XRD for the crystalline nature and interplanar spacing, SEM/EDS for the detection of the surface morphology and elemental composition, TEM for the analysis of surface morphology of GO nanosheets, SPM (AFM) for average thickness and area of GO nanosheets formed and TGA for thermal behavior. FT-IR spectra of graphite and as-synthesized GO were obtained using Perkin Elmer Spectrum RX-I Fourier Transform Infrared Spectrophotometer. XRD studies of graphite and GO_a were carried out using PANalytical XPERT-PRO (NDP) X- Ray Diffractometer using CuKα radiation (λ = 1.54 Å) and 2θ in the range from 10° - 50°. SEM/EDS of graphite and GO_a were acquired using JEOL JSM-6610LV. TEM studies were carried out using Technai G2 20 S-TWIN FEI Netherlands Transmission Electron Microscope. AFM analysis was carried out using NT-MDT-INTEGRA Scanning Probe Microscope. For TEM characterization, diluted suspensions of Graphite and GO_a were prepared using ultrasonication technique and deposited on a carbon support grid and allowed to dry in air. For AFM analysis, a very dilute GO suspension was put on a small piece of monocrystalline silicon (5 mm × 5 mm × 0.45 mm) and dried it in a vacuum oven at 50 °C.

2.4. Size- reduction of synthesized GO by ball milling and characterization of size- reduced GO

The synthesized GO sample was subjected to planetary ball milling in propanol medium (i.e. wet milling) using Zirconia balls on a planetary ball mill Retsch PM 200 at rotation speed of about 200 rpm to obtain the GO having even more degree of fineness of nanosheets. Any incorporation of structural defects such as formation of curved nanosheets and warping during ball milling was carefully controlled using optimized milling duration of about 16 hours.[36]

Since contamination is expected on continuous milling when high rotational speed is employed, the milling process was interrupted at frequent intervals. The obtained product was

made free of solvent with repeated washings with deionized water. Then the sample was again vacuum dried completely and the size- reduced GO sample was marked as GO_b. The GO_b sample was also characterized using FTIR, XRD, TEM, AFM and TGA techniques so as to monitor the surface functional groups post ball milling, to view the morphology of size - reduced nanosheets and to confirm the size – reduction of GO nanosheets.

2.5. Fabrication of GO - Cement Nanocomposites (GO-CNCs)

Cement and standard sand were mixed in a proportion of 1:3 by mass and mixed well to obtain a uniform and homogenous dry mixture. Calculated amount of water was mixed thoroughly to the prepared dry mixture of cement and sand. Preparation of control mix (without GO) was carried out both in the absence and presence of PC (0.1% by wt. of cement) so as to investigate the influence of PC on its workability and to confirm whether PC had any significant strength contribution or not in the present investigation. Simultaneously, aqueous dispersions of GO_a were prepared in the presence of superplasticizer using ultrasonic energy for 1 hour for each mix. The energy of ultrasonic shock waves is extremely high which exfoliates the nanosheets and thereby breaks the agglomerates, if formed any. The sonicator was operated at constant amplitude of 50% so as to deliver energy of 2000 J/min at cycles of 20 sec in order to prevent overheating of specimens. The dispersions were prepared using different concentrations of GO_a i.e. 0.125%, 0.25%, 0.50% and 1.00% by wt. of cement, with amount of PC ranging between 0.12 to 0.40 (% by wt. of cement). The water/cement ratio (w/c) of all the mixes was kept constant at 0.45. The dispersions were also prepared using same concentrations of GO_b sample but the amount of PC was slightly enhanced ranging from 0.20 to 0.50 (% by wt. of cement). The dosage of PC was decided on the basis of ensuring required workability of mortar mixes. The paste made was considered workable only if it filled the moulds without bleeding and segregation. The details of mix design of test specimens are shown in Table 3. The prepared dispersions of both types of GO were manually mixed with homogeneous cement-sand mixture for about 5 minutes. The fresh mortar pastes were filled in standard size moulds with dimensions 70.5 mm × 70.5 mm × 70.5 mm to prepare samples for testing of compressive strength. Before filling up fresh mortar pastes into the moulds, the moulds were cleaned, brushed and oiled properly. The filled moulds were subjected to electric vibrations at a rate of 2600 rpm to ensure the complete compaction of mortar pastes. Three cubes were prepared for control mix and for

each concentration of GO incorporated into the mix so as to reduce the error. The filled moulds were then kept for complete setting for 24 hours and hardened nanocomposites samples were demoulded and kept for curing in a curing tank under standard conditions at a constant temperature of 27±2 °C with an attached temperature regulator and 90% relative humidity until testing.

Table 3 Mix design of test specimens

2.6. Determination of mechanical properties of GO_a cement nanocomposites (GO_a-CNCs) and GO_b cement nanocomposites (GO_b-CNCs)

The nanocomposites were evaluated for their mechanical behavior by testing their compressive strength using 200 tons capacity Compression Testing Machine (CTM) HEICO 49.55. The surface dry samples were tested at increasing curing times of 7, 14 and 28 days as per BIS requirements i.e. BIS: 269: 1976. The cubic samples were positioned at right angles to that of the casting position while testing. Axis of specimens was carefully aligned with the center of thrust of the plates. A gradual load was applied and increased to a constant loading rate of 5.2 N/mm^2 until the failure of sample took place. Average value of three cubes was reported as compressive strength to reduce error.

2.7. Microstructural analysis and crystalline investigations of GO-CNCs

The fracture surfaces of GO cement nanocomposites (GO-CNCs) were characterized for their microstructure using Ultra Plus Carl Zeiss FE- SEM (Field Emission Scanning Electron Microscopy) at increasing curing times of 7, 14 and 28 days. All the samples were gold coated using sputtering technique prior to microscopy analysis. Pore structure of the samples cured for 28 days was analyzed using Intrusion Porosimeter. The size of sample chosen for analysis was kept close to 1 cm and kept for drying at 100°C in vacuum oven for about 24 hours. To reduce error, three repetitions were carried out on each sample.

XRD patterns for the study of various crystalline phases after 28 days curing were acquired using PANalytical XPERT-PRO (NDP) X- Ray Diffractometer using CuKα radiation (λ = 1.54 Å) operated at 40 mA and 45 kV. Incident beam divergence slit was fixed at 1.00° and all scans were measured over an angular range of 10° to 70° 2θ with the step size 0.0170° 2θ, resulting in scan step time of 20.95 sec. Samples were powdered finely and sieved to remove coarse large

granules prior to XRD characterization. Powdered samples were produced by grinding. The XRD results were interpreted to obtain the crystallographic information for the cement hydration products, such as the type and relative content of the hydration crystals formed as well as the cement phases undergoing consumption. The rate of increase or decrease of the relative content of a particular crystalline phase was calculated from the following equation:

$$Rate\ of\ increase\ or\ decrease\ of\ a\ crystalline\ phase\ (\%) = \frac{I_{GO} - I_{Control}}{I_{GO}} \times 100 \qquad (1)$$

where, I_{GO} and $I_{Control}$ are the intensities of crystalline phase in GO-CNC and control respectively. It was ensured that the weight of a particular powdered sample for XRD characterization be constant.

3. Results and Discussion

3.1. Structural characterization of GO_a and GO_b

FT-IR spectra of precursor Graphite powder (GP), as - synthesized Graphene Oxide (GO_a) and size – reduced Graphene Oxide (GO_b) are shown in Fig. 2a. From the spectra, it is clear that treatment of graphite precursor with oxidizing agents leads to the surface functionalization of graphite flakes. For GP, the absorption peak for -C=C- stretch was observed at *1629* cm^{-1}, showing the presence of alkenic bonds in graphite. In case of GO_a, a prominent peak at *3300* cm^{-1} is attributed to presence of hydroxyl groups (-OH) in GO and peak at *1735* cm^{-1} shows the presence of carbonyl group (C=O), confirming the –COOH group. A peak at *937* cm^{-1} is characteristic of the presence of C-O stretch in epoxides. The C-O-C stretch is also confirmed by the absorption peak at *1026* cm^{-1}. Appearance of well – defined and sharp pointed peak at *1160* cm^{-1} is an evidence for SO_3 asymmetric stretch confirming the incorporation of sulphonic group ($-SO_3H$) in GO. Presence of aromatic double bonds is confirmed by the absorption peak at *1631* cm^{-1}. These results justify the presence of incorporated oxygen- containing functional groups in GO nanosheets. From IR spectrum of GO_b, it was concluded that absorption peaks corresponding to similar functional groups (-OH, –COOH, $-SO_3H$, C=O) were also observed which confirms the successful preservation of functional moieties even after ball – milling.

The XRD patterns of GP, GO_a and GO_b are shown in Fig. 2b. The characteristic diffraction peak (002) of GP at 26.54° with interpalanar spacing 3.354 Å disappeared in the XRD spectrum of GO. An additional peak at 13.7° was observed, which was attributed to (001) diffraction peak of GO. The broadening of peak in XRD spectrum of GO depicts the increased interplanar

spacing due to incorporation of functional moieties. These moieties get embedded in between the layers of graphitic sheets and thereby the spacing between adjacent sheets increases. The line broadening for the characteristic diffraction peak observed in case of GO_a is attributed to smaller size of nanosheets which further gets broadened in XRD of GO_b. It is also mentioned that optimized ball milling duration in present study is around 15.5 to 16 hrs. When milling duration reaches the optimized duration, ball milled GO had a similar chemical nature to that of original GO as can be seen in Fig. 2b. The line broadening also indicates exfoliation of interlayers of GO.

Fig. 2c represents the possible scheme for the conversion of raw material graphite powder into graphite oxide in the presence of oxidizing agents. Oxidation process leads to the increase in the interplanar spacing on account of incorporation of oxygen containing functional groups.

Fig. 2 (a) FTIR spectra of precursor graphite powder (GP), as- synthesized graphite oxide (GO_a) and ball - milled graphite oxide (GO_b) (b) XRD patterns of GP, GO_a and GO_b (c) Schematic representation showing the surface functionalization of GP leading to formation of GO with increased interlayer spacing

Fig. 3a shows the SEM micrograph of GP precursor indicating the flaky nature of the material. Fig. 3b represents the SEM image of as- synthesized GO_a showing the crumpling on the surface and wrinkling of the membranous nanosheets. This occurs as a result of attachment of various functional groups over the surface of GO while oxidative treatment of graphite. Table 4 summarizes the elemental composition of the starting material and synthesized GO after EDAX analysis.

Fig. 3 (a) SEM image of GP (b) SEM image of as - synthesized GO

Table 4 Elemental compositions of GP and as - synthesized GO after EDAX analysis

The TEM images of GP and GO_a are shown in Fig. 4a and 4b respectively, revealing the surface morphologies of graphite flakes and GO_a nanosheets at higher magnification. The difference between the morphology of GP and GO_a lies in the fact that GP is thick- layered as indicated from transparency and has no wrinkled surface whereas GO_a possesses a wrinkling surface appearing as crumpled paper and is relatively thin-layered which is attributed to better exfoliation of surface functionalized GO nanosheets. The TEM image for GO_b nanosheets is also shown in Fig. 4c. The image shows the GO nanosheets which are smaller in size as compared to

GO_a nanosheets. There are some visible smaller fragments of GO nanosheets. TEM results also confirm the absence of any other distinct nanostructures and a successful formation of GO fragments after ball milling.

Fig. 4 TEM images of (a) GP precursor (b) As - synthesized GO_a nanosheets (c) Size - reduced GO_b nanosheets

The AFM images of synthesized GO_a nanosheets and ball - milled GO_b nanosheets are shown in Fig. 5. Fig. 5a represents the 2-D topography of GO_a nanosheets. Average sheet thickness (height) is shown in Fig. 5b. Fig. 5c shows the 3-D view of GO_a nanosheets. The thickness of GO_a nanosheets prepared from GP precursor is 14 nm having an average sheet size of 0.9 μm (900 nm). The AFM results of GO_b are shown in Fig. 5 (d-f), where it was observed that size of GO sheets undergo size reduction so that the sheets have average size of 0.1 μm (100 nm) and average sheet thickness of 3 nm. The smaller GO_b nanosheets can be viewed in Fig. 5d (however the sheets are very small in their size) and number of nanosheets has also increased. The sheet height can be seen in Fig. 5e and a better 3-D view of nanosheets can be seen in Fig. 5f. It is therefore apparent that original GO nanosheets get reduced in size from 900 nm to 100 nm after subjection to ball milling process.

Fig. 5 (a) AFM image 2-D topography of GO_a nanosheets (b) Height profile of GO_a (c) 3-D view of GO_a (d) AFM image 2-D topography of size - reduced GO_b nanosheets (smallest lamellae shown with arrows) (e) Height profile of GO_b (f) 3-D view of GO_b

The thermogravimetric (TGA) curves for the starting material and the GO nanosheets are shown in Fig. 6a. As can be seen from the TGA results, the thermal behavior of both types of GO nanosheets indicates significant weight loss with increase in temperature. The GO begins to lose moisture even below 100°C, which is attributed to loss of the water molecules adsorbed or trapped in between GO layers. Another major loss can be observed around 200°C which is due to the elimination of gaseous products such as CO and CO_2. When the temperature > 250°C, a continuous weight loss was observed till it reached 600°C. In between a sudden loss around 350°C could possibly be related to loss of >C=O components and bent curvature might be due to subsequent accommodation of C-O components or groups. Comparing the TGA curves of GO_a and GO_b, it is apparent that initial weight loss is rapid in the latter case because the heat

accessibility and thermal penetration is assumed to be more on high surface area smaller GO nanosheets. Since GO_b is exfoliated, it is indicated that it shows more water loss with a resulting increased initial weight loss at 100°C. To investigate the degradation kinetics, DTG curves were also plotted as shown in Fig. 6b. The DTG plots reveal that there GO_b has relatively higher area under the peak possibly due to more weight loss but there is no significant variation in comparison to GO_a.

Fig. 6 (a) Thermogravimetric (TGA) curves; and (b) Differential thermogravimetric (DTG) curves of GP, GO_a and GO_b

3.2. Determination of mechanical properties of control mix and GO - cement nanocomposites (GO-CNCs)

Further, to evaluate the effectiveness of both types of GO nanosheets as the reinforcing materials in cement mortar, the fabricated GO-CNCs were tested for their compressive strength at increasing curing times of 7, 14 and 28 days. The results of compressive strength of the GO_a and GO_b nanocomposites compared to control mix tested are shown in Table 5a and Table 5b respectively. Since the effect of superplasticizer had to be removed from the present analysis, the percentage increase in compressive strength of control mix with use of PC with respect to control mix without use of PC is represented in Fig. 7a. Graphical representation of the results of two types of nanocomposites at different concentration levels of GO_a and GO_b with increasing curing times is shown in Fig. 7b and 7c respectively. Here, the comparison of compressive strength is shown with the control mix made using PC. It is observed that the variation in compressive strength of control mix in the absence and presence of PC was insignificant at increasing curing times. This observation indicates that contribution of PC used in present study towards strength enhancement is negligible. Surface of PC has anionic charge owing to presence of carboxylate units which help to promote electrostatic repulsions between cement and sand grains and the reinforcing material added, thereby improving the workability by creating suitable dispersions. From the compressive strength results of GO-CNCs, it was also observed that as the concentration of GO nanosheets (% by wt. of cement) was increased, the compressive strength also increased significantly at different curing times of 7, 14 and 28 days. In case of GO_a - cement nanocomposites, the maximum percentage increase in the compressive strength after 28 days of curing was shown by the highest concentration of GO_a incorporated in cement mortar

matrix (i.e. 63.3%) with respect to the control sample (unreinforced counterpart) containing no GO nanosheets.

In contrast, the GO_b cement nanocomposites had shown even higher improvement in the mechanical properties. The percentage increase in this case ranged from 35% to 86% for different concentrations of GO_b nanosheets added into matrix, compared to the control sample.

Table 5a Compressive strength results of GO_a - Cement Nanocomposites

Table 5b Compressive strength results of GO_b - Cement Nanocomposites

Fig. 7 (a) Percentage increase in compressive strength of control with use of PC and; Graphical representation of compressive strength results of (b) GO_a-CNCs (c) GO_b-CNCs; at different concentrations of GO_a or GO_b with increasing curing time

The major factor responsible for improvement in the mechanical strength of GO-CNCs is the strong interfacial bonding of both types of GO nanosheets with the cement matrix which is attributed to the surface functionalized nature of GO. Another factor is the high nucleating activity of high surface area of the nanosheets, over which hydration reactions of cement compounds (i.e. C_3S, C_2S, C_3A and C_4AF) can proceed more feasibly. The probability for the chemical reactions is further enhanced in case of smaller nanosheets of GO_b, since they possess higher surface area to mass ratio in comparison to GO_a nanosheets. More number of smaller nanosheets get uniformly distributed as well as dispersed throughout the matrix. Higher surface area and more number of nanosheets increases the number of active sites both for interfacial bonding as well as nucleation of cement hydrates. Although PC has active carboxylate sites but its presence merely ensures required workability and creates stable dispersions by creating a layer of common charge over cement grains thereby allowing for electrostatic repulsions. As observed for control mix, role of PC has minimal contribution towards strength enhancement which could be neglected. In addition, it is postulated that reduction of w/c ratio along with use of PC could enhance the compressive strength. For this, w/c was also kept constant in present investigation. Since GO synthesized in the present investigation has far greater oxygenated-functionality on its surface (about 53%), therefore, it is postulated that the interfacial covalent bonding between cement particles and GO nanosheets are solely responsible for improvement in strength. Even if weight to weight percentage of GO nanosheets and PC are considered, it is obvious that functionality and large surface of GO sheets is more accessible to the hydrating

particles. Nanosheets can act as nuclei for cement phases, further promoting cement hydration due to their high reactivity, as nanoreinforcement.

The improvement in strength is further correlated to the microstructure of the GO cement composites, discussed in the next section of this paper.

3.3. Microstructure of two types of GO - cement nanocomposites (GO-CNCs)

To investigate the effect of GO nanosheets on the microstructural properties of cement mortar matrix, SEM images were taken from the fracture surfaces of plain mortar sample at 7, 14 and 28 days. The micrographs are shown in Fig. 8a, Fig. 8b and Fig. 8c respectively. It was observed that the hydration crystals obtained in case of plain mortar are loosely bound together and poorly dense. There are numerous crystals which are mostly *acicular* shaped (needle – like) and appear dis - arrayed throughout the matrix. These crystals are responsible for the brittleness of the material since they grow in random directions. The loose structure of hydration products is quite prominent in early hydration ages of 7 and 14 days. The major crystalline hydrates are of *ettringite* (Aft), *monosulphates* (Afm) and *portlandite* (CH). Apart from these crystals, a semi – crystalline hydrate i.e. *calcium – silicate – hydrate* (C-S-H) can exist which may be *fibrillar* or *flaky* or in the form of gel in the cementitious matrix. The control samples fabricated in the presence of superplasticizer were also observed for their microstructure and it was observed that crystals undergo modification in their morphology but still lack an ordered arrangement at increasing curing times of 7, 14 and 28 days which can be observed respectively in Fig. 8d, Fig. 8e, Fig. 8f. This is in correspondence with the observed mechanical properties of control mix in the absence and presence of PC.

Fig. 9 shows the SEM images of fracture surfaces of GO – cement nanocomposites (GO-CNCs) containing GO concentration level of 0.125% (by wt. of cement) at curing time of 7, 14 and 28 days. The images depict an improved microstructure upon addition of GO nanosheets (both GO_a and GO_b) in comparison to that of control sample. The cement hydrates form a compact pattern of *prismatic* or *columnar* geometry at 7 days curing (Fig. 9a and Fig. 9b). However, the relative content of these crystals is apparently higher for the composite incorporating the smaller sized GO_b nanosheets (Fig. 9b). At 14 days, it seems that these columnar crystals undergo fusion to form compacted microstructure (Fig. 9c and Fig. 9d). Since the chemical reactivity of GO_b nanosheets is proposed to be higher, the crystals begin to adopt

the fused geometry at a faster rate (Fig. 9d), whereas in Fig. 13c, the crystals still tend to remain in columnar geometry which shows that the rates of hydration lag behind by some rate in these nanocomposites. For 28 days old GO-CNCs (Fig. 9e and Fig. 9f), a *platy* structure is achieved and these plates are merged strongly in GO_b cement nanocomposites.

Fig. 10 represents the SEM images for GO-CNCs containing 0.25% GO nanosheets at curing time of 7, 14 and 28 days. As seen in Fig. 10a and Fig. 10b, the SEM images at 7 days curing show numerous *columnar* (bar – shaped) cement hydrates (Fig. 10b) emerging out of C-S-H phase in comparison to rather seated hydrates observed in Fig. 10a. It is observed that increase in GO concentration from 0.125% to 0.25% (by wt. of cement) does not significantly alter the basic crystal geometry at 7 days of curing. As we go for 14 days, the SEM observations respectively show fusing cement hydrates for GO_a composites (Fig. 10c) whereas a beaded type of continuous arrayed pattern is seen in case of GO_b composites (Fig. 10d). At 28 days (Fig. 10e and Fig. 10f) old specimens, the crystalline products have a tendency to adhere together leading to the formation of *hexagonal* plates. These hexagonal plates are smaller in case of GO_a nanocomposites when compared to larger and adhered ones in GO_b nanocomposites and this can be owed to higher surface area due to more number of nanosheets available in the latter case for similar concentration of GO. This makes the easy availability of nucleating sites with large number for huge growth of cement hydrates.

The SEM images for the fracture surfaces of GO-CNCs containing 0.50% GO (by wt. of cement) are shown in Fig. 11. As the concentration of GO_a is increased to 0.50%, it is seen that hydrates attain *tentacular* shapes and these tentacles are highly abundant in number, packed up very closely to give a *bushy* - type microstructure (Fig. 11a) after 7 days. These crystals gradually fuse together to give rise to thickened cement hydrates in case of nanocomposites having GO_a (Fig. 11c) on further curing. For those containing GO_b nanosheets, the cement hydrates are rather *leaflet* or *lamellar* - shaped (Fig. 11b). These lamellae are clustered together at the base and emerge out of the nucleating sheets of GO. The lamellae are divergent in nature at their tips (Fig. 11b) and as the hydration accelerates, the size of these lamellae expands to gradually fill up the cement matrix (Fig. 11d). At 28 days curing, Fig. 11e and Fig. 11f represent the microstructure of nanocomposites revealing the *octahedral* hydrates and *wedgy* - *polyhedral* hydrates for GO_a and GO_b cement nanocomposites respectively. It is proposed that increase in

concentration level of GO to 0.50% in cementitious matrix makes the crystal habits turn from *hexagonal* to *octahedral* or *polyhedral* geometry.

On further increasing GO concentration level to 1.00%, there are stacked rows of cement hydrates which are thick bars (Fig. 12a) and these appear beautifully in ordered arrays layered one above the other (Fig. 12b). On moving to 14 days cured specimens, GO_a nanocomposites achieve geometry where the *sectored - octahedral* plates are formed (Fig. 12c). In Fig. 12d, these plates are stacked and contain interwoven network of crystals. As the composites reach 28 days of curing, the sectored portion gradually attains a *sphenoid* habit (Fig. 12e) and the stacked plates attain a giant mass of *blocky - polyhedral* geometry (Fig. 12f).

Fig. 8 SEM images of plain mortar without GO after (a) 7 days (b) 14 days (c) 28 days curing; and SEM images of plain mortar without GO in presence of PC after (e) 7 days (f) 14 days (f) 28 days curing

Fig. 9 SEM images of 0.125% (bwoc) GO_a nanocomposites and GO_b nanocomposites after (a & b) 7 days (c & d) 14 days (e & f) 28 days curing respectively

Fig. 10 SEM images of 0.25% (bwoc) GO_a nanocomposites and GO_b nanocomposites after (a & b) 7 days (c & d) 14 days (e & f) 28 days curing respectively

Fig. 11 SEM images of 0.50% (bwoc) GO_a nanocomposites and GO_b nanocomposites after (a & b) 7 days (c & d) 14 days (e & f) 28 days curing respectively

Fig. 12 SEM images of 1.00% (bwoc) GO_a nanocomposites and GO_b nanocomposites after (a & b) 7 days (c & d) 14 days (e & f) 28 days curing respectively

3.4. Pore structure of GO – cement nanocomposites (GO-CNCs)

The porosity plays an important role in influencing the mechanical properties of cement-based materials. Compressive strength of cementitious materials is directly related to its pore structure. As explained in previous section, addition of both types of GO nanosheets significantly enhances the compressive strength of the cement mortar matrix by regulating the geometries of cement hydrates. To investigate the influence of GO_a and GO_b nanosheets in cementitious matrix, pore structure was analyzed in both cases and the results are shown in Table 6. As clearly indicated from the results, concentration of GO as well as sheet size of GO have a considerable effect on the obtained values. As the concentration level of GO_a or GO_b is increased from 0.125% to 1.00%, the porosity goes on decreasing. This is attributed to pore - filling effect of nano-sized

GO. Further, small-sized GO_b nanosheets promote better reduction in porosity owing to their finer sizes. It is therefore postulated that addition of more finer nanosheets help to reduce the pores in better way. Total pore area, median pore diameter and total porosity are reduced with incorporation of GO_a and GO_b nanosheets. All possible voids and pores are filled up which finally leads to an enhancement in the compressive strength.

Table 6 Porosity of control mix and GO-CNCs after 28 days of curing

The combined results of microstructure and porosity show that increase in percentage of GO from 0.125% to 1% remarkably improves the compressive strength due to its sufficient dispersion in cementitious matrix. If the material had not been properly dispersed, it would act as stress raisers in the pores and voids of the matrix and consequently would have degraded the mechanical performance. The SEM observations and percentage porosity results also revealed that a porous and loose interfacial zone was initially present between the cement matrix and fine aggregates in the control mix without GO nanosheets, while a dense interfacial zone was present when GO addition formed a denser microstructure with less porous structure. As hydration progressed, the interfacial zone between cement and sand aggregates was gradually replaced by growing amount of hydrates over pore-filling GO nanosheets.

3.5. X- Ray Diffraction for crystalline and hydration behavior in GO - cement nanocomposites (GO-CNCs)

XRD was used to determine the qualitative and quantitative interpretation of various crystalline phases present in cement mortar matrix and for evaluation of early hydration reactions taking place.[31, 37] XRD patterns for GO_a cement nanocomposites and GO_b cement nanocomposites are shown in Fig. 13a and Fig. 13b respectively. The amounts of major crystalline phase i.e. calcium hydroxide was used as an indication of degree of hydration. The peak for portlandite (i.e. CH or $Ca(OH)_2$) appears at positions 18.2°, 34.2°, 47.1° and 50.1°.[37-39] The intensities of the peaks corresponding to CH crystals were found to increase with increase in concentration of GO in the cement mortar matrix. CH peaks at position 18.2°, 34.1° and 50.1° gradually sharpens (maximum in 1.00% GO-CNC) with increasing concentration of GO suggesting an increase of hydration in nanocomposites. The control sample has relatively lesser quantity of portlandite phase. Since the calcium – silicate – hydrate (C-S-H) gel is the amorphous cement hydrate,

therefore, its detection quantitatively from the XRD spectra is limited. However, its quantity can be estimated by the increasing quantities of CH crystallites which mostly precipitate out as hexagonal plate like prisms and these crystallites grow in different directions to achieve polyhedral geometry. The amount of the precipitation of these crystallites increases as a result of increased hydration reactions of the Alite (C_3S) and Belite (C_2S) phases.[40] Alite can have different polymorphic forms such as Monoclinic, Triclinic, Rhombohedral and these forms show peaks between 2θ ranging between 51° - 52° (i.e. 51.3°, 51.5° and 51.8°). For plain mortar, these peaks show high contents of Alite (Tricalcium Silicate) and gradually show disappearance when GO is increased to higher concentrations. A major peak also appears at 29.3° for monoclinic C_3S[40] in plain mortar with sharp intensity which slowly reduces in terms of intensity with slight variation in case of GO-CNCs. The diffractograms also show relative consumption in the amount of Belite (Dicalcium Silicate) with increasing amounts of GO as reinforcing material. The major quartz peak at 2θ = 26.7° [41] is observed to possess equal intensity in both GO_a and GO_b nanocomposites. It is assumed that the equivalent intensity of this major Qz peak is related to equal proportion of sand (SiO_2) used in each mix. Tricalcium Aluminate or C_3A appears strongly in case of sample without any GO at position 2θ = 33.1° for the Cubic polymorph and an adjacent peak at positions 32.9° for its Orthorhombic polymorph.[40] C_3A reactivity is explained from the overlap of two polymorphic forms in case of nanocomposites as well as fall in their intensities. Relative decrease in amounts of C_4AF (Tetracalcium Aluminoferrite) at 2θ = 23.3° can also be correlated to higher hydration rates of the nanocomposites. Table 7 shows the rate of increase/decrease of different major crystalline phases in control sample and GO-CNCs, as calculated using equation (1).

Fig. 13 XRD patterns (a) GO_a - Cement Nanocomposites (b) GO_b - Cement Nanocomposites (at different GO_a and GO_b concentrations) after 28 days curing

Table 7 Rate of increase or decrease of different crystalline phases in control and GO-CNCs

Apart from these major characteristic features of the diffractograms, it was observed that both the control sample and GO-CNCs show similarity in showing the presence of common cement compounds (i.e. Calcium silicates and calcium aluminates) but the amounts of these compounds certainly vary depending upon the crystallinity of the material.

Comparison of XRD patterns of GO_a nanocomposites and GO_b nanocomposites indicates that the relative quantities of cement hydration products (CH, Aft and Afm) are higher in GO_b nanocomposites. In this case, the growth rate of crystallites post hydration reactions is proportional to the number of nucleating sites available for cement compounds to undergo hydration.

3.6. Strengthening mechanism of GO monolayers acting as templates for interfacial covalent bonding

It is well known that monolayers of GO are decorated with various oxygenated moieties which are responsible for their increased chemical reactivities. The GO monolayers act as templates where the role of active sites is well performed by the oxygen - containing functional groups (which is 53% in present study). These consequently adsorb the chemical compounds present in the cement as soon as a solvating medium is provided in the presence of water. The components of cement such as C_2S, C_3S, C_3A tend to undergo hydration over the surface of GO layers which is further strengthened by the strong interfacial bonding taking place between functionalized templates and the hydrated cementitious phases (Fig. 14a).

Comparing the chemical reactivities of as - synthesized GO_a and GO_b monolayers, it can be postulated that ball - milling induces an effective increase in the number of GO sheets for a fixed concentration which was incorporated into cement mortar matrix and this consequently allowed better dispersion of GO_b sheets over a large area throughout the matrix in a uniform manner. Since the number of nanosheets had increased, the cement compounds had availability of larger number of GO templates with active sites where the hydration reactions proceeded at a faster rate. Presence of individual and scattered monolayers of GO was also capable of avoiding the steric hindrance among growing hydration crystals that could arise if the molecules of silicates and aluminates had been undergoing hydration over single GO monolayer. A schematic has been outlined in Fig. 14b showing the growth of cement hydrates leading to formation of different crystal geometries. Two cases can be assumed to compare the strengthening mechanism of two types of GO: In the first, hydration crystals grow over a single available GO nanosheet of 900 nm average size and in the other, same crystals are growing over nine GO nanosheets of 100 nm average size each (assuming that ball milling converts one nanosheet into nine nanosheets), with equal number of oxygenated moieties in each of the case. The SEM, porosity and XRD results

also confirm that GO nanosheets with smaller size have a greater effect on the quantity of cement hydrates, their crystal shapes and geometries, and a wider distribution of cement hydration crystals throughout the matrix, which result in good strengthening effects.

Fig. 14 (a) Schematic showing interfacial bonding between surface functional groups of GO monolayer and hydrated phases of cementitious matrix (b) Schematic showing conversion of growing cement hydrates with definite shapes into fused geometry over GO_a and GO_b templates with active sites

4. Conclusions

Incorporation of as – synthesized larger GO nanosheets and ball – milled smaller GO nanosheets was carried out in the present investigation. It was concluded from the results that addition of both the types of GO significantly improves the compressive strength of cement based materials by controlling their microstructure and the amounts and shapes of cement hydrates. The shapes of crystals could be columnar, platy, tentacular, polyhedral, etc. Ball – milling was found to be an effective tool to carry out the fragmentation of single GO nanosheet into large number of GO nanosheets which had a higher surface area as indicated by better strengthening effects of ball – milled GO. The technique can be used as a substitute to exfoliation by ultrasonication which requires small amounts of material every time to be exfoliated.

Moreover, the amount of relative increase in mechanical properties is dependent upon the concentration of GO added as reinforcing material in cement mortar matrix. The results also indicated that GO being surface functionalized in nature had no dispersion issues otherwise any possible formation of agglomerates would badly degrade the mechanical performance of composites.

The present research provides a pathway for researchers to exploit GO as a low – cost and strong reinforcing material in cement based materials and has future scope of various practical applications.

Acknowledgements

One of the authors Snigdha Sharma would like acknowledge Ministry of Human Resource Development (MHRD) for providing financial assistance to carry out the research. The authors gratefully acknowledge Dr B R Ambedkar National Institute of Technology, Jalandhar for

providing the suitable laboratory facilities to carry out this research. The authors would also like to acknowledge Indian Institute of Technology (IIT), Roorkee (Uttrakhand), India for providing characterization facilities like FE-SEM, EDAX, AFM, TEM and Indian Institute of Technology (IIT), Ropar (Punjab), India for providing XRD facility.

Notes and References

1 J. M. Berthelot and J. L. Robert, *J. Engng. Mech*., 1990, **116**, 587-604.

2 S. Chakraborty, S. P. Kundu, A. Roy, B. Adhikari and S. B. Majumder, *Ind. Eng. Chem. Res.,* 2013, **52**, 1252-1260.

3 E. M. Golafshani, A. Rahai and M. H. Sebt, *Constr. Build. Mater.*, 2014, **61**, 230-240.

4 S. Tokgoz, C. Dundar and A. K. Tanrikulu, *J. Constr. Steel Res.*, 2014, **74**, 98-107.

5 J. P. Won, B. T. Hong, T. J. Choi, S. J. Lee and J. W. Kang, *Compos. Struct.*, 2012, **94**, 1443-1449.

6 D. Y. Yoo, J. H. Lee and Y. S. Yoon, *Compos. Struct.*, 2013, **106**, 742-753.

7 C. Abeysinghe, D. P. Thambiratnam and N. J. Perera, *Compos. Struct*., 2013, **95**, 179-190.

8 S. Marikunte, C. Aldea and S. P. Shah, *Adv. Cem. Based Mater.*, 1997, **5**, 100-108.

9 X. Shu, R. K. Graham, B. Huang B and E. G. Burdette, *Mater. Design*, 2015, **65**, 1222-1228.

10 G. Xu and D. J. Hannant, *Cement Concr. Compos.*, 1991, **3**, 95-106.

11 M. Uysal and H. Tanyildizi, *Constr. Build. Mater.*, 2012, **27**, 404-414.

12 E. M. Bezerra, A. P. Joaquim, Jr. H. Savastano, V. M. John and V. M. Agopyan, *Cement Concr. Compos.*, 2006, **28**, 555-563.

13 F. Sanchez and C. Ince, *Compos. Sci. Technol.*, 2009, **69**, 1310-1318.

14 H. K. Kim, I. W. Nam and H. K. Lee, *Compos. Struct.*, 2014, **107**, 60-69.

15 S. Musso, J .M. Tulliani, G. Ferro, A. Tagliaferro, *Compos. Sci. Technol.*, 2009, **69**, 1985-1990.

16 R. K. Abu Al - Rub, A. I. Ashour and B. M. Tyson, *Constr. Build. Mater.*, 2012, **35**, 647-655.

17 M. S. Morsy, S. H. Alsayed and M. Aqel, *Constr. Build. Mater.*, 2011, **25**, 145-149.

18 S. Parveen, S. Rana and Fangueiro R., J. Nanomater. 2013; 2013 Article ID 710175, http://dx.doi.org/10.1155/2013/710175.

19 X. L. Xie, Y. W. Mai and X. P. Zhou, *Mater. Sci. Eng. Rep*., 2005, **49**, 89-112.

20 G. Y. Li, P. M. Wang and X. Zhao, *Carbon*, 2005, **43**, 1239-1245.

21 G. Y. Li, P. M. Wang and X. Zhao, *Cem. Concr. Compos.*, 2007, **29**, 377-382.

22 A. Yazdanbakhsh, Z. C. Grasley, B. Tyson and R. K. Abu Al- Rub, *In: ACI Fall 2009 Convention, November 267*, 2009, 31-34.

23 Y. W. Zhu, S. Murali, W. W. Cai, X. S. Li, J. W. Suk, J. R. Potts and R. S. Ruoff., *Adv. Mater.,* 2010, **22**, 3906-3924.

24 S. Stankovich, D. A. Dikin, R. D. Piner, K. A. Kohlhaas, A. Kleinhammes, Y. Jia, Y. Wu, S. T. Nguyen and R. S. Ruoff, *Carbon*, 2007, **45**, 1558-1665.

25 D. Konios, M. M. Stylianakis, E. Stratakis and E. Kymakis, *J. Colloid Interf. Sci*., 2014, **430**, 108-112.

26 J. I. Paredes, S. Villar-Rodil, A. Martinez-Alonso and J. M. D. Tascon, *Langmuir,* 2008, **24**, 10560-10564.

27 D. Han, L. Yan, W. Chen and W. Li, *Carbohydr. Polym.*, 2011, **83**, 653-658.

28 J. Lin, P. Zhang, C. Zheng, X. Wu, T. Mao, M. Zhu, H. Wang, D. Feng, S. Qian and X. Cai, *Appl. Surf. Sci.*, 2014, **316**, 114-123.

29 M. Ionita, M. A. Pandele and H. Iovu, *Carbohydr. Polym.*, 2013, **94**, 339-344.

30 M. Ionita, M. A. Pandele, L. Crica and L. Pilan, *Compos. Part B: Eng.*, 2014, **59**, 133-139.

31 S. Lv, Y. Ma, C. Qiu, T. Sun, J. Liu and Q. Zhou, *Constr. Build. Mater.*, 2013, **49**, 121-127.

32 S. M. Hong, J. J. Park, E K. Park, K. Y. Kim, J. G. Lee, M. K. Lee, C. K. Rhee and J. K. Lee, *Powder Technology*, 2015, **274**, 393-401.

33 H. Panjiar, R .P Gakkhar and B. S. S. Daniel, *Powder Technology*, 2015, **275**, 25-29.

34 H. Q. Li, Y. G. Wang, C. X. Wang and Y. Y. Xia, *J. Power Sources*, 2008, **185**, 176-182.

35 W. Zhao, M. Fang, F. Wu, H. Wu, L. Wang L and G. Chen, *J. Mater. Chem.*, 2010, **20**, 5817-5819.

36 D. Zhang, X. Zhang, X. Sun, H. Zhang, C. Wang and Y. Ma, *Electrochimica Acta*, 2013, **109**, 874-880.

37 R. Snellings, A. Salze and K. L. Scrivener, *Cem. Concr. Res.*, 2014, **64**, 89-98.

38 F. Kontoleontos, P. Tsakiridis, A. Marinos, N. Katsiotis, V. Kaloidas and M. Katsioti, *Constr. Build. Mater.,* 2012, **35**, 347-360.

39 M. A. Trezza, *Mat. Res*., 2007, **10**, 331-334.

40 R. Jadhav and N. C. Debnath, *Bull. Mater. Sci.*, 2011, **34**, 1137-1150.

41 F. Rendell, R. Jauberthie and M. Grantham, *Deteriorated Concrete: Inspection and Physicochemical Analysis*, 2000, 110, ebook ISBN 978-0-7277-3758-8, DOI: 10.1680/dc.31197.

List of Tables

Table 1 Chemical Properties of OPC

Contents	**Test Value (%)**
CaO	64.90
SiO_2	21.49
SO_3	0.70
Al_2O_3	4.21
Fe_2O_3	3.50
MgO	2.90
Insoluble residue	1.10
Total loss on Ignition	1.20

Table 2 Specifications of three grades of Indian Standard Sand

Grade of Sand	Type of Standard Sand	Particle Size Range (mm)	Amount used in study (%)
Grade I	Coarse	2 mm to 1mm	33.33%
Grade II	Medium	1 mm to 0.5 mm	33.33%
Grade III	Fine	0.5 mm to 0.09 mm	33.33%

Table 3 Mix design of test specimens

Test Specimens	Concentration of GO_a/GO_b (% by wt. of cement)	w/c ratio	Amount of PC (% by wt. of cement)
Control	0	0.45	0.1
GO_a-CNC	0.125	0.45	0.12
GO_a-CNC	0.25	0.45	0.2
GO_a-CNC	0.50	0.45	0.3
GO_a-CNC	1.00	0.45	0.4
GO_b-CNC	0.125	0.45	0.2
GO_b-CNC	0.25	0.45	0.3
GO_b-CNC	0.50	0.45	0.4
GO_b-CNC	1.00	0.45	0.5

Table 4 Elemental compositions of GP and as - synthesized GO after EDAX analysis

	Elemental percentage (%)			
	Carbon	Oxygen	Sulphur	Manganese
GP	92.59	6.4	1.01	0
GO	41.34	53.59	4.66	0.34

Table 5a Compressive strength results of GO_a - Cement Nanocomposites

GO_a concentration (%)	**Compressive strength (MPa) with increasing curing time/ % age increase relative to unreinforced counterpart**		
	7 days	14 days	28 days
0	16.2/0	18.4/0	24.8/0
0.125	20.9/29.0	23.9/29.9	29.7/19.6
0.25	21.4/32.0	26.2/42.4	34.5/39.1
0.50	26.1/61.1	32.2/75.0	35.5/43.1
1.00	30.9/90.7	36.2/96.7	40.5/63.3

Footnote: GO_a-CNCs were fabricated at w/c ratio of 0.45 with PC 0.12% to 0.4% (by wt.% of cement) and control with PC 0.1% by mixing 260 g cement, 780 g Indian standard sand, 117 ml water and certain concentration of GO_a (% by wt. of cement).

Table 5b Compressive strength results of GO_b - Cement Nanocomposites

GO_b concentration (%)	**Compressive strength (MPa) with increasing curing time/ % age increase relative to unreinforced counterpart**		
	7 days	14 days	28 days
0	16.2	18.4	24.8
0.125	24.9/53.7	28.0/52.2	33.5/35.1
0.25	26.2/61.7	32.7/77.7	36.2/45.9
0.50	30.5/88.3	33.6/82.6	40.8/64.5
1.00	32.5/100.6	39.4/114.1	46.2/86.3

Footnote: GO_b-CNCs were fabricated at w/c ratio of 0.45 with PC 0.125% to 0.4% (by wt.% of cement) and control with PC 0.1% by mixing 260 g cement, 780 g Indian standard sand, 117 ml water and certain concentration of GO_b (% by wt. of cement).

Table 6 Porosity of control mix and GO-CNCs after 28 days of curing

	Total porosity (%)								
		0.125%		0.25%		0.50%		1.00%	
	Control	GO_a	GO_b	GO_a	GO_b	GO_a	GO_b	GO_a	GO_b
Total pore area (m^2/g)	20.65	17.20	16.88	15.10	13.60	13.35	11.91	10.34	10.10
Median Pore Diameter (nm)	29.40	24.46	22.79	22.00	17.81	16.77	12.60	12.30	9.56
Total porosity (%)	25.21	21.28	20.69	19.80	16.30	14.42	12.28	11.30	10.61

Table 7 Percentage increase or decrease in different crystalline phases in control and GO-CNCs

Concentration of GO (% by wt. of cement)	CH (%)		C_3S (%)		C_2S (%)		Aft (%)	
	GO_a	GO_b	GO_a	GO_b	GO_a	GO_b	GO_a	GO_b
0 (Control)	36	36	52.3	52.3	31.8	31.8	16.4	16.4
0.125	30.2	37.5	48.1	41.0	30.4	27	21.2	18.0
0.25	39.6	66.2	36.6	40.0	29.0	29.4	28.3	13.6
0.50	83.4	87.2	58.1	38.1	28.5	22.0	25.2	56.0
1.00	86.2	94.6	24.8	22.4	21.2	18.3	53.7	33.1

Figures

(Number of figures: 14)

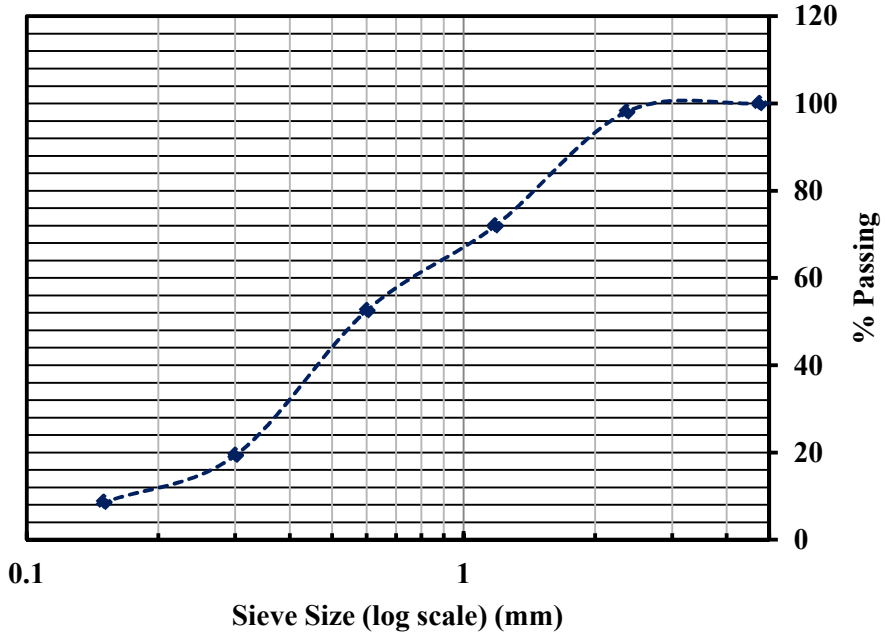

Fig. 1 Sieve analysis of fine aggregates (equal proportion of Grade I, II and III) showing particle size distribution

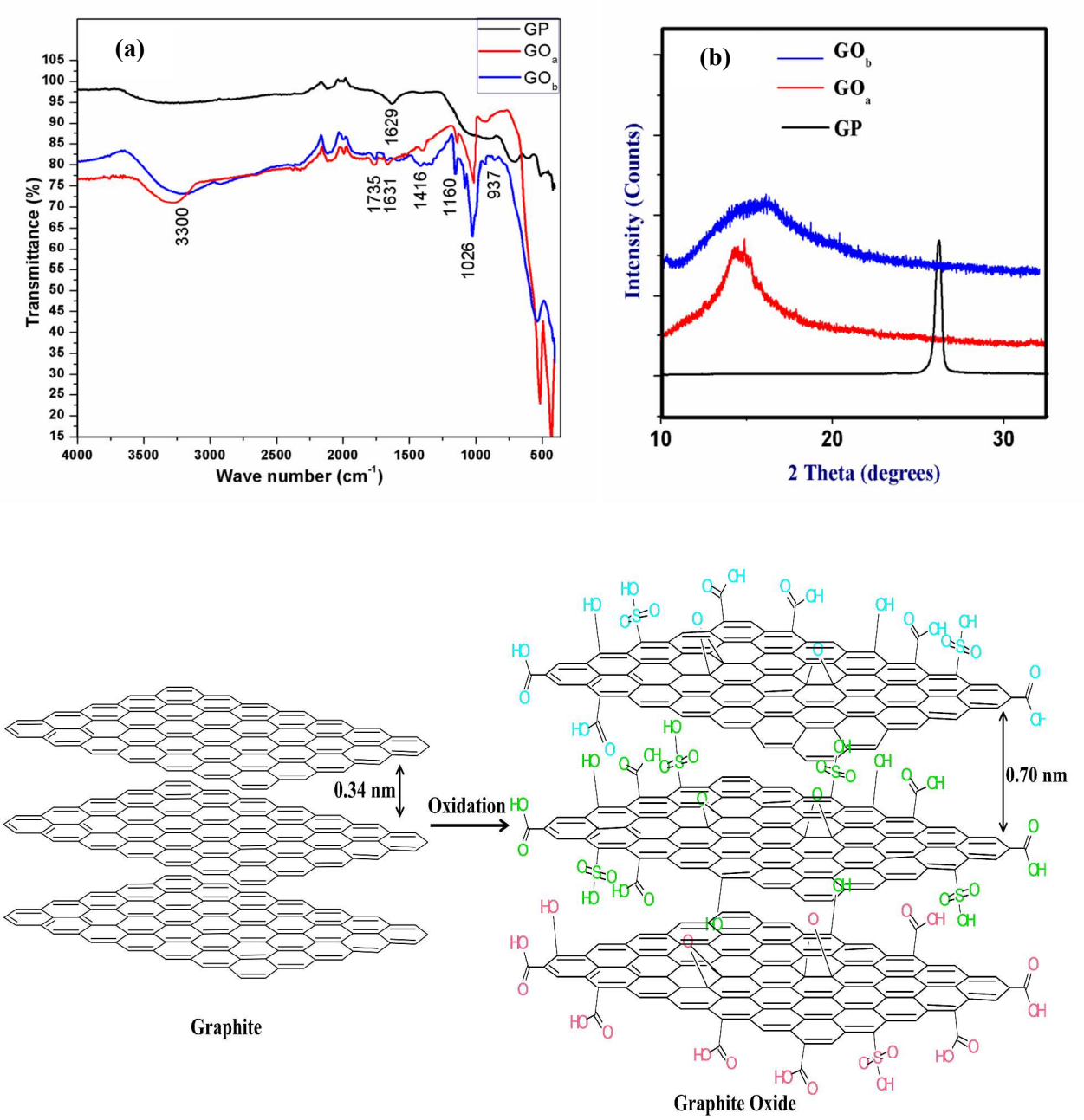

Fig. 2 (a) FTIR spectra of precursor graphite powder (GP), as- synthesized graphite oxide (GO_a) and ball - milled graphite oxide (GO_b) (b) XRD patterns of GP, GO_a and GO_b (c) Schematic representation showing the surface functionalization of GP leading to formation of GO with increased interlayer spacing

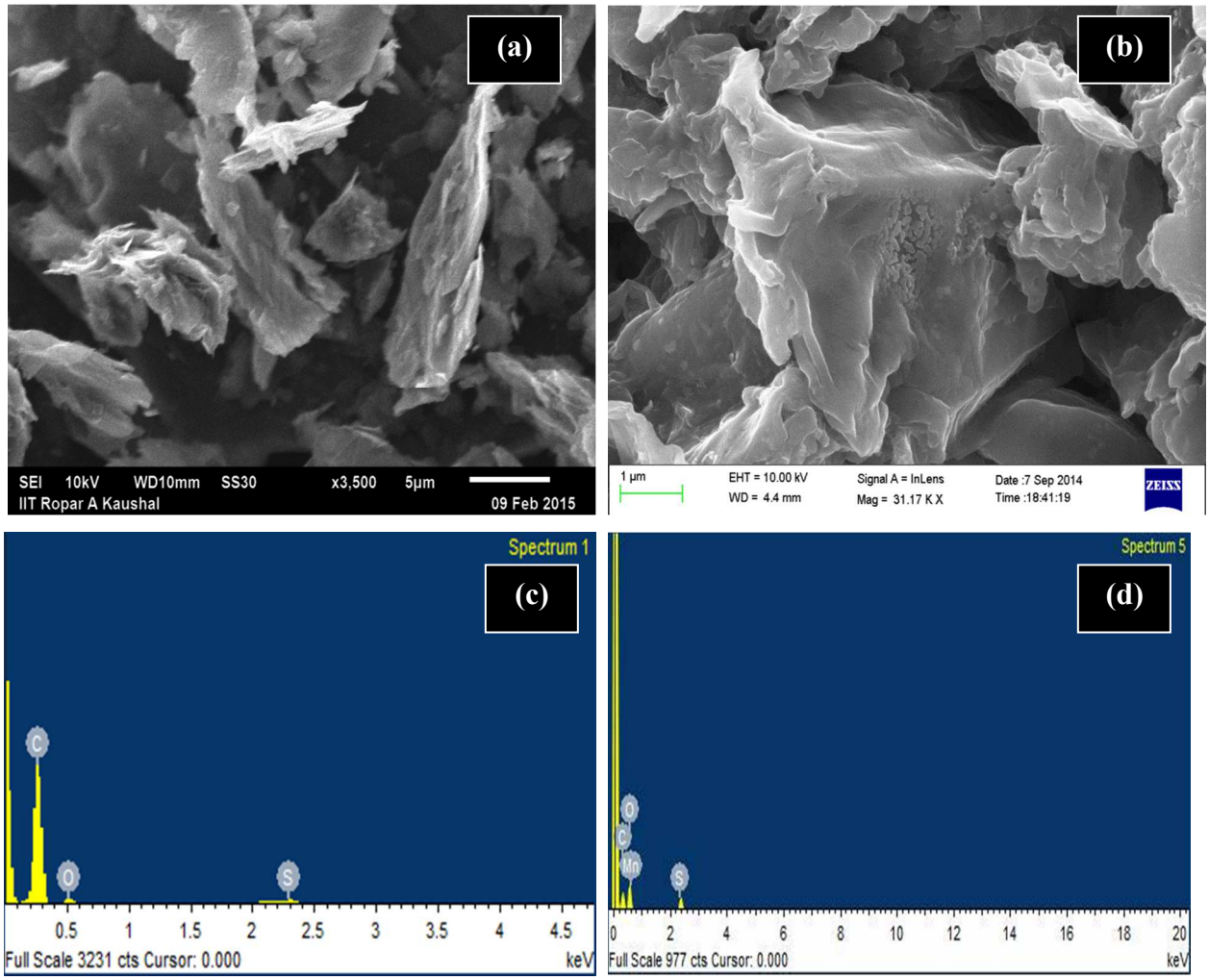

Fig. 3 (a) SEM image of GP (b) SEM image of as - synthesized GO (c) EDAX spectrum of GP (d) EDAX spectrum of GO

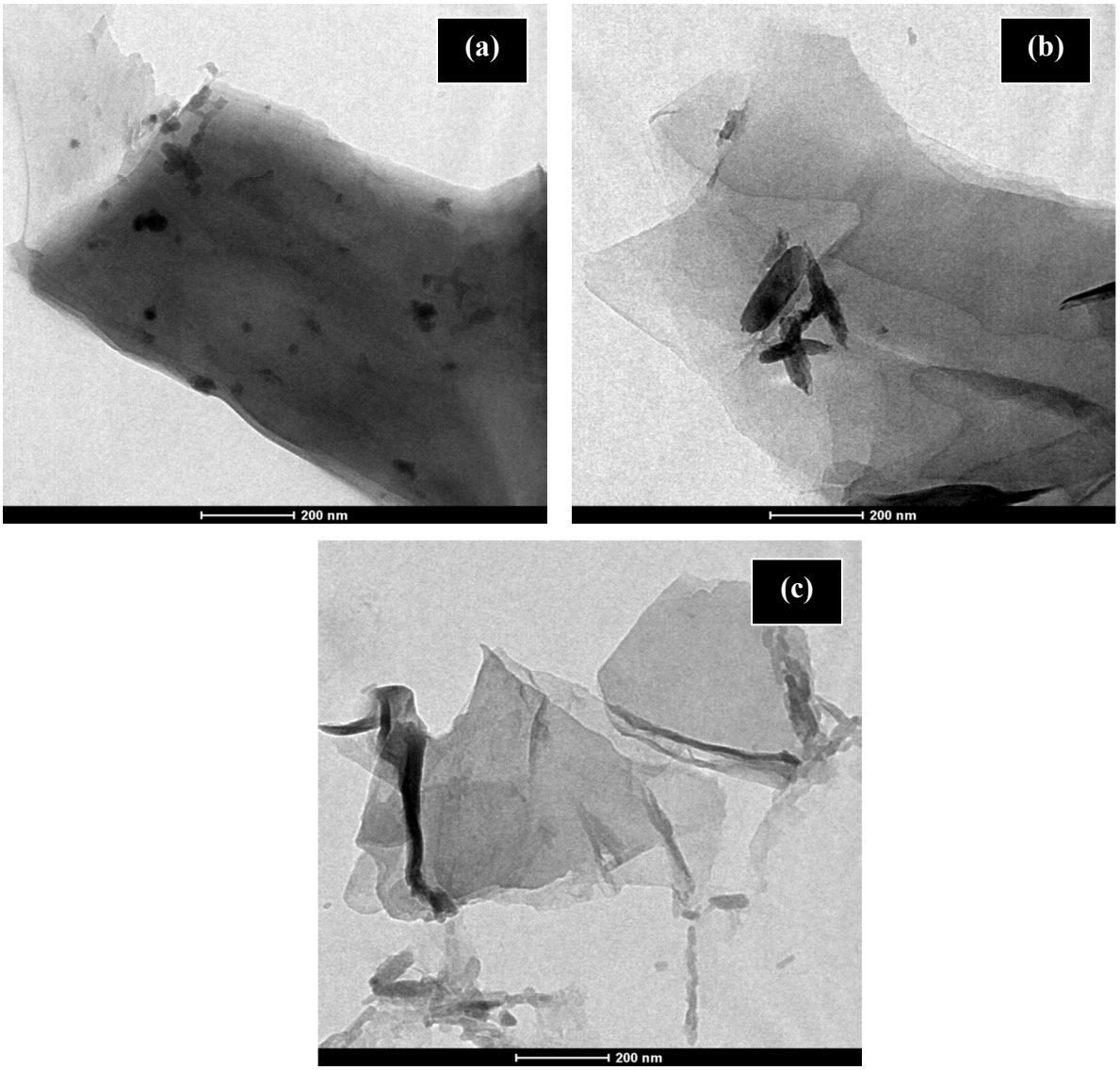

Fig. 4 TEM images of (a) GP precursor (b) As – synthesized GO_a nanosheets (c) Size – reduced GO_b nanosheets

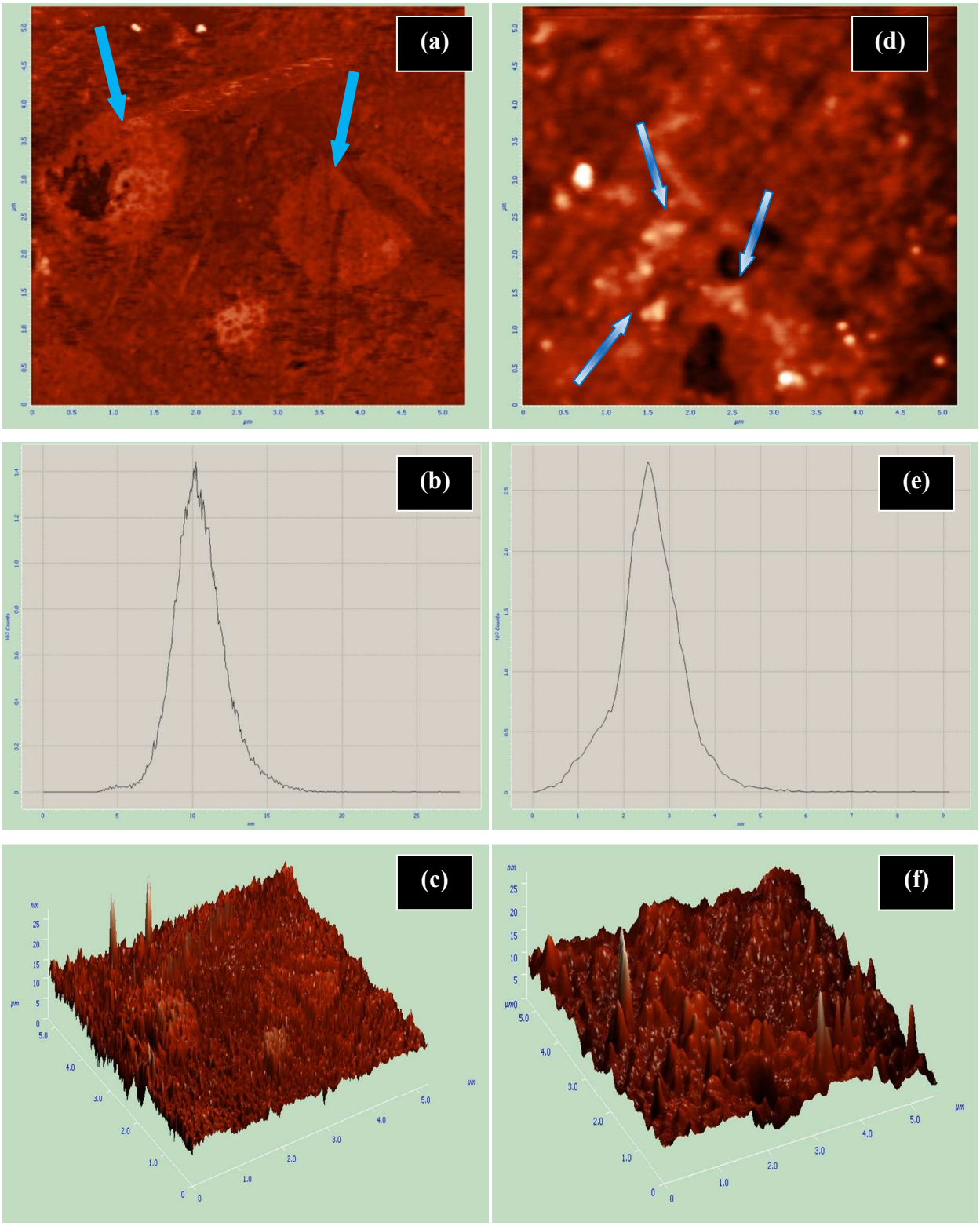

Fig. 5 (a) AFM image 2-D topography of GO_a nanosheets (b) Height profile of GO_a (c) 3-D view of GO_a (d) AFM image 2-D topography of size - reduced GO_b nanosheets (smallest lamellae shown with arrows) (e) Height profile of GO_b (f) 3-D view of GO_b

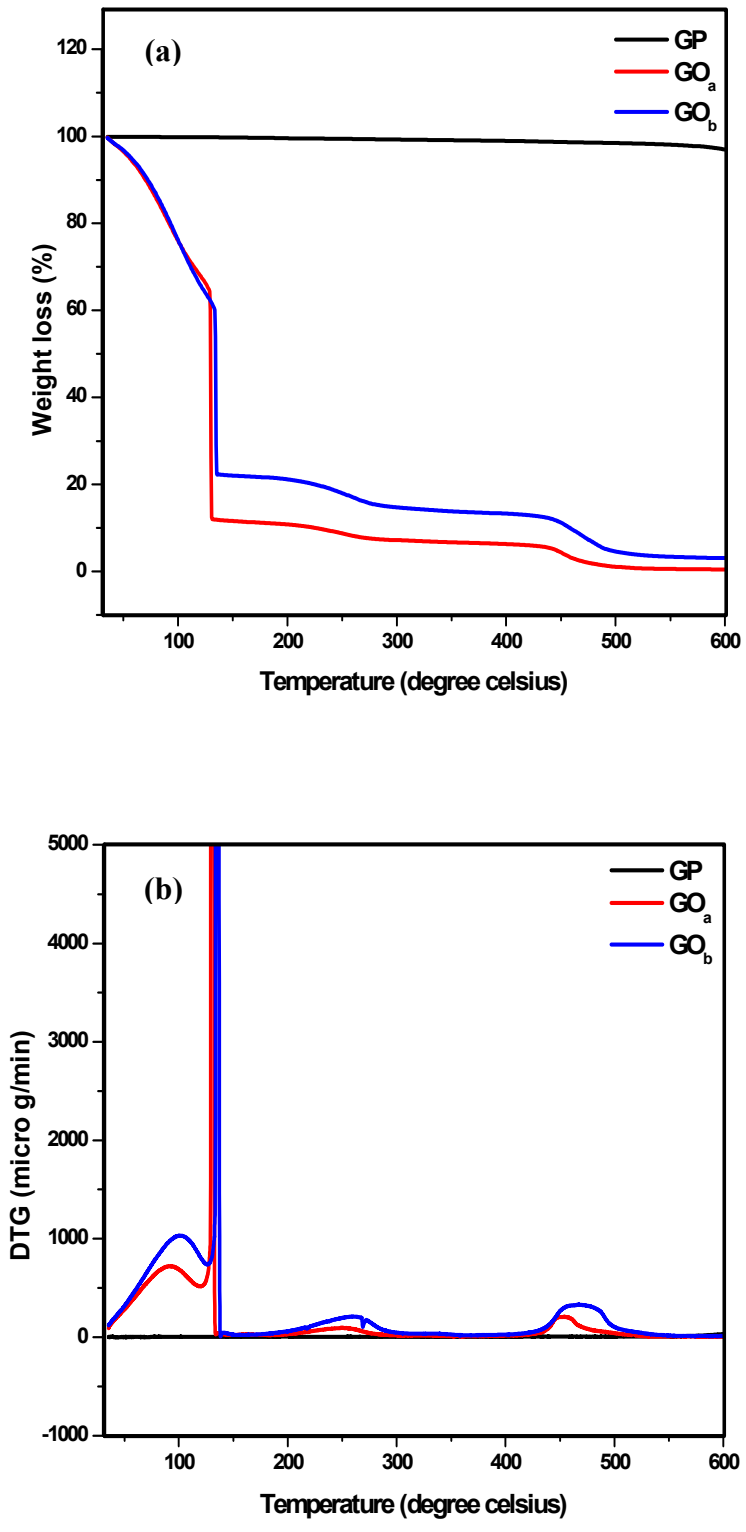

Fig. 6 (a) Thermogravimetric (TGA) curves of GP, GO_a and GO_b (b) Differential Thermogravimetric Analysis (DTG) of GP, GO_a and GO_b

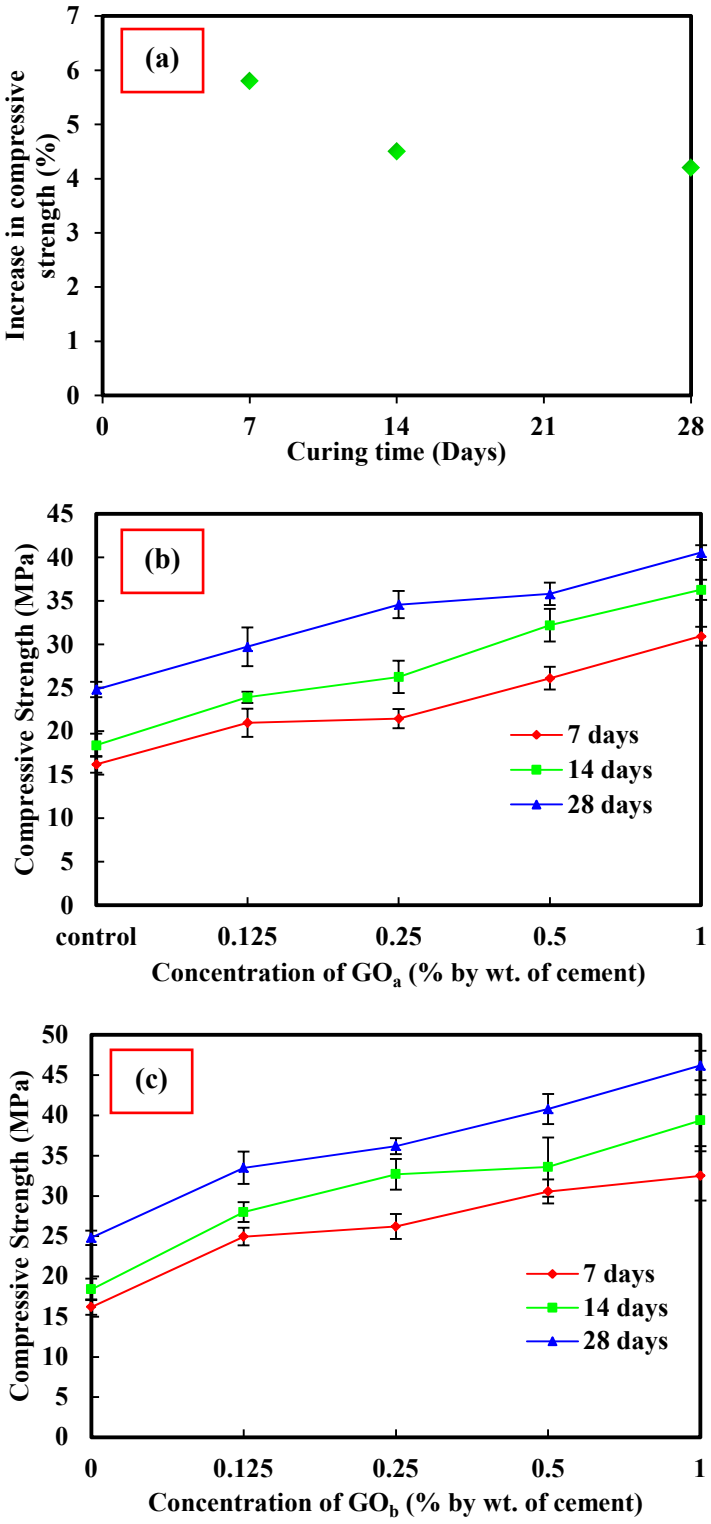

Fig. 7 (a) Percentage increase in compressive strength of control with use of PC and; Graphical representation of compressive strength results of (b) GO_a-CNCs (c) GO_b-CNCs; at different concentrations of GO_a or GO_b with increasing curing time

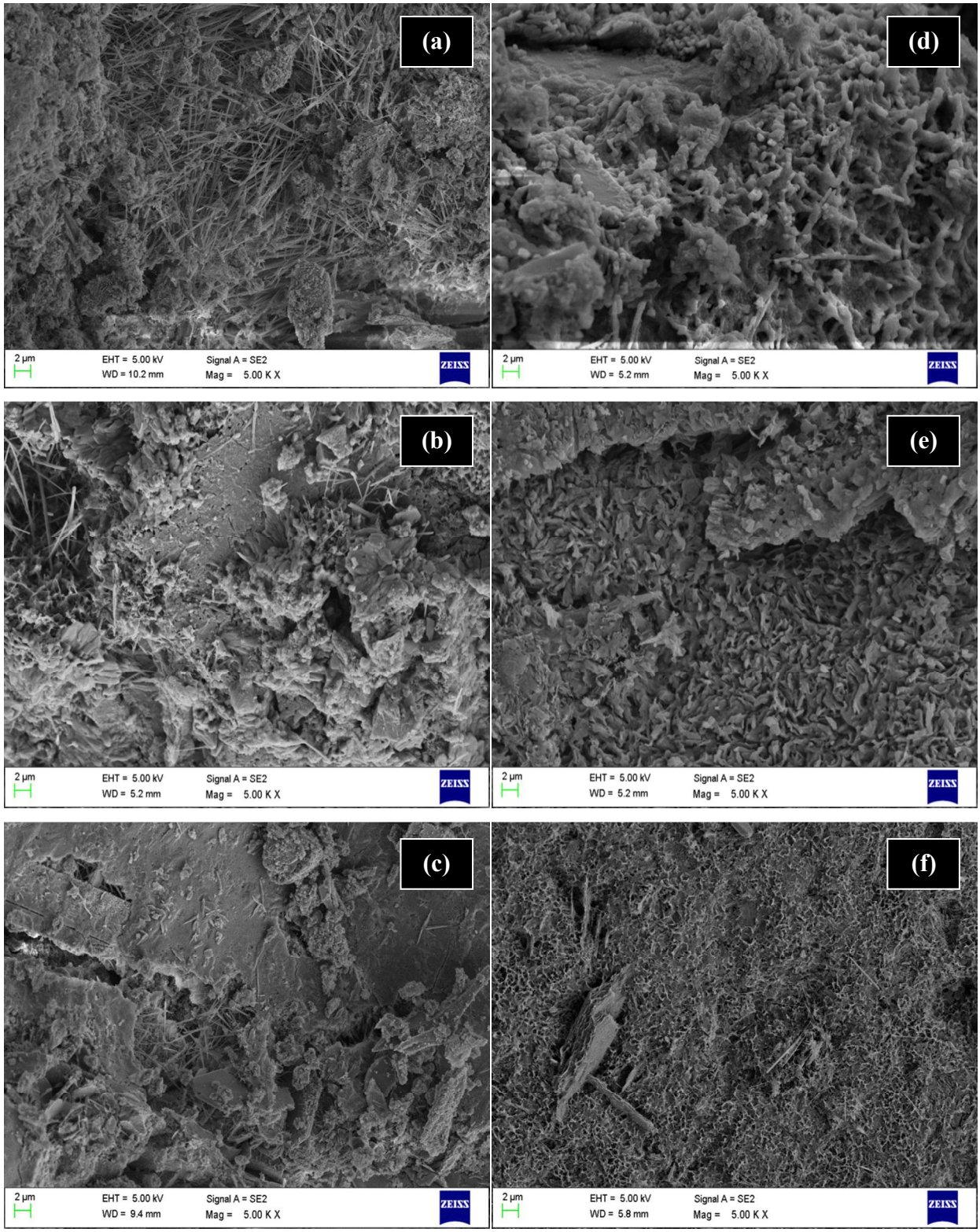

Fig. 8 SEM images of plain mortar without GO after (a) 7 days (b) 14 days (c) 28 days curing; and SEM images of plain mortar without GO in presence of PC (d) 7 days (e) 14 days (f) 28 days curing

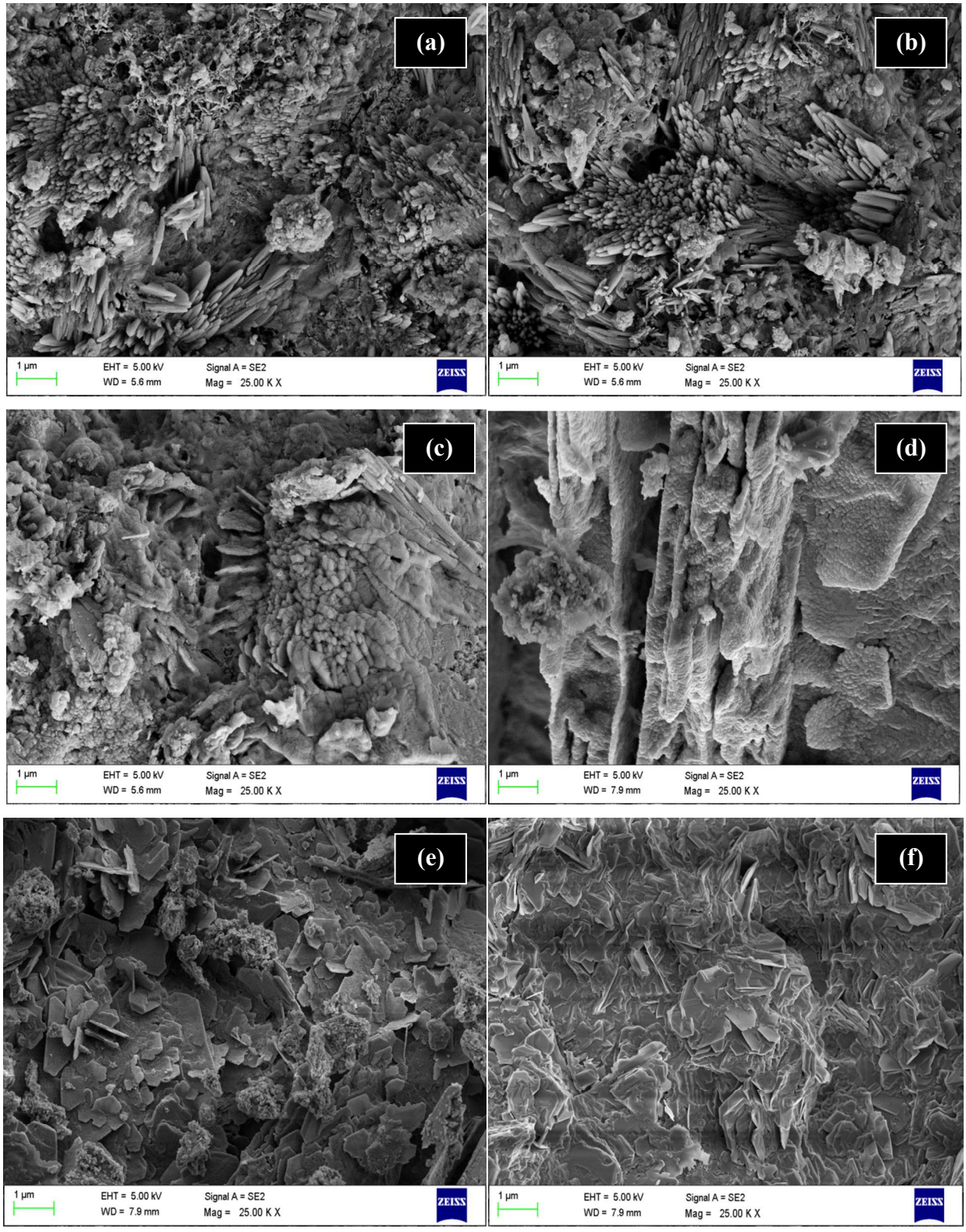

Fig. 9 SEM images of 0.125% (bwoc) GO_a nanocomposites and GO_b nanocomposites after (a & b) 7 days (c & d) 14 days (e & f) 28 days curing respectively

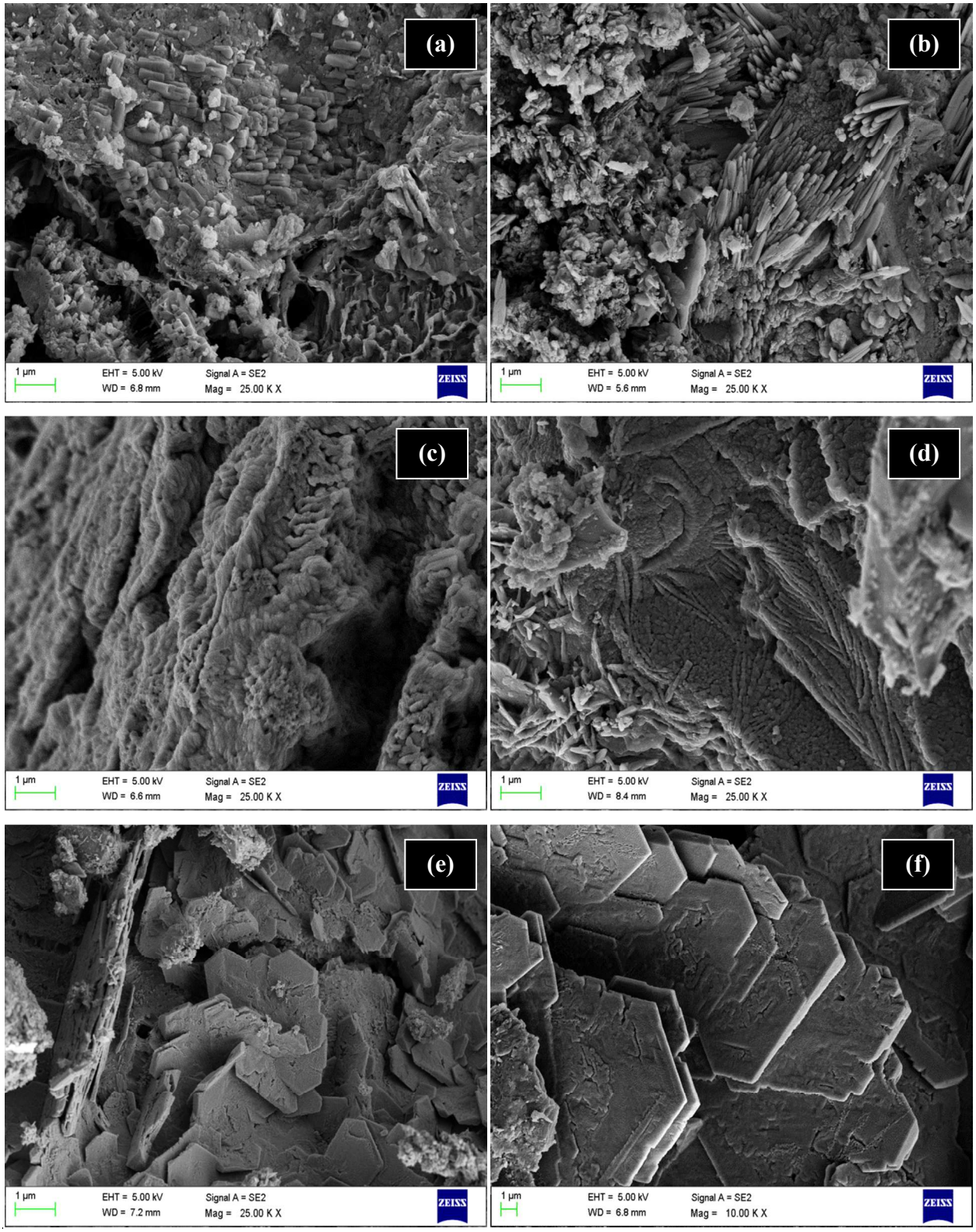

Fig. 10 SEM images of 0.25% (bwoc) GO_a nanocomposites and GO_b nanocomposites after (a & b) 7 days (c & d) 14 days (e & f) 28 days curing respectively

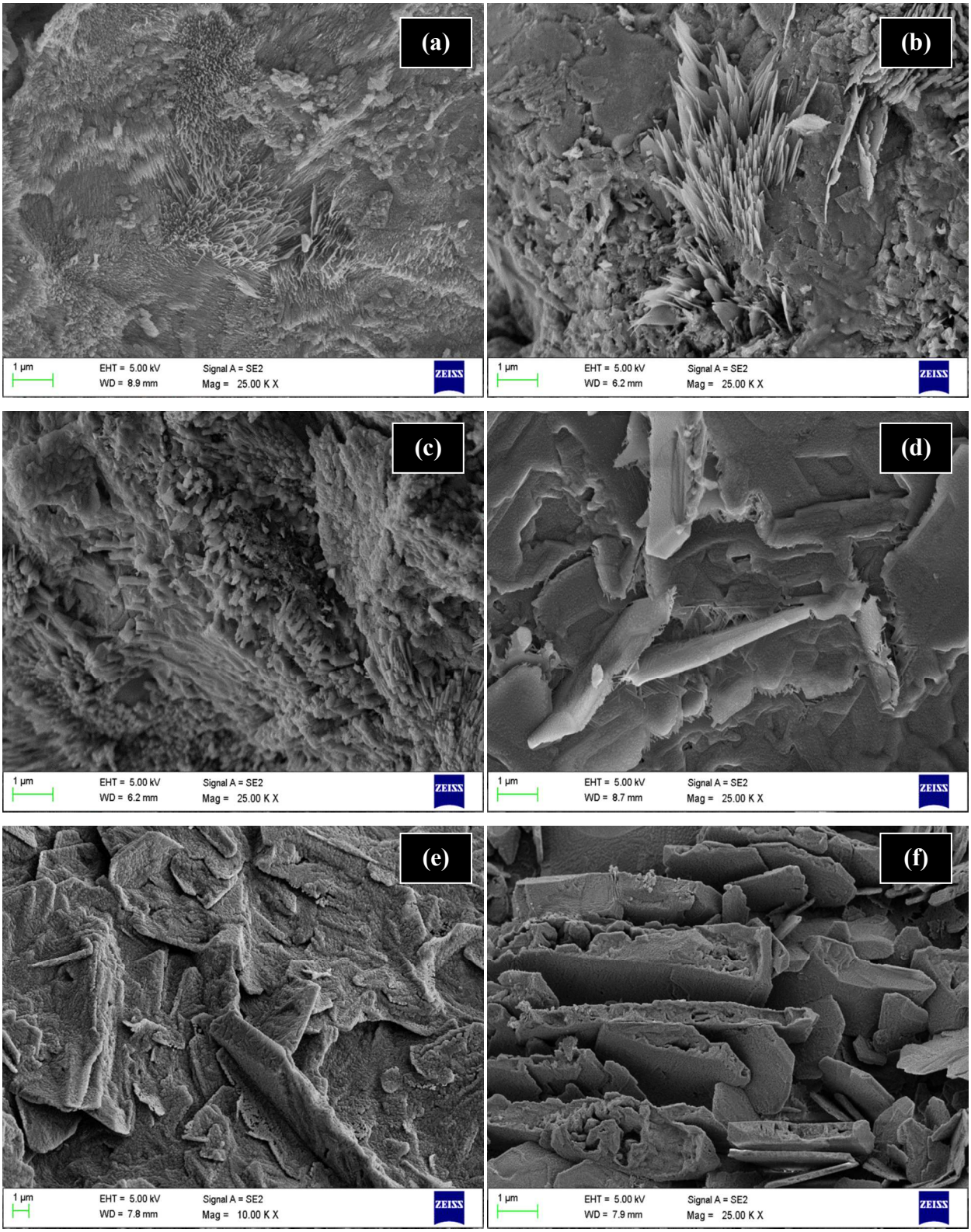

Fig. 11 SEM images of 0.50% (bwoc) GO_a nanocomposites and GO_b nanocomposites after (a & b) 7 days (c & d) 14 days (e & f) 28 days curing respectively

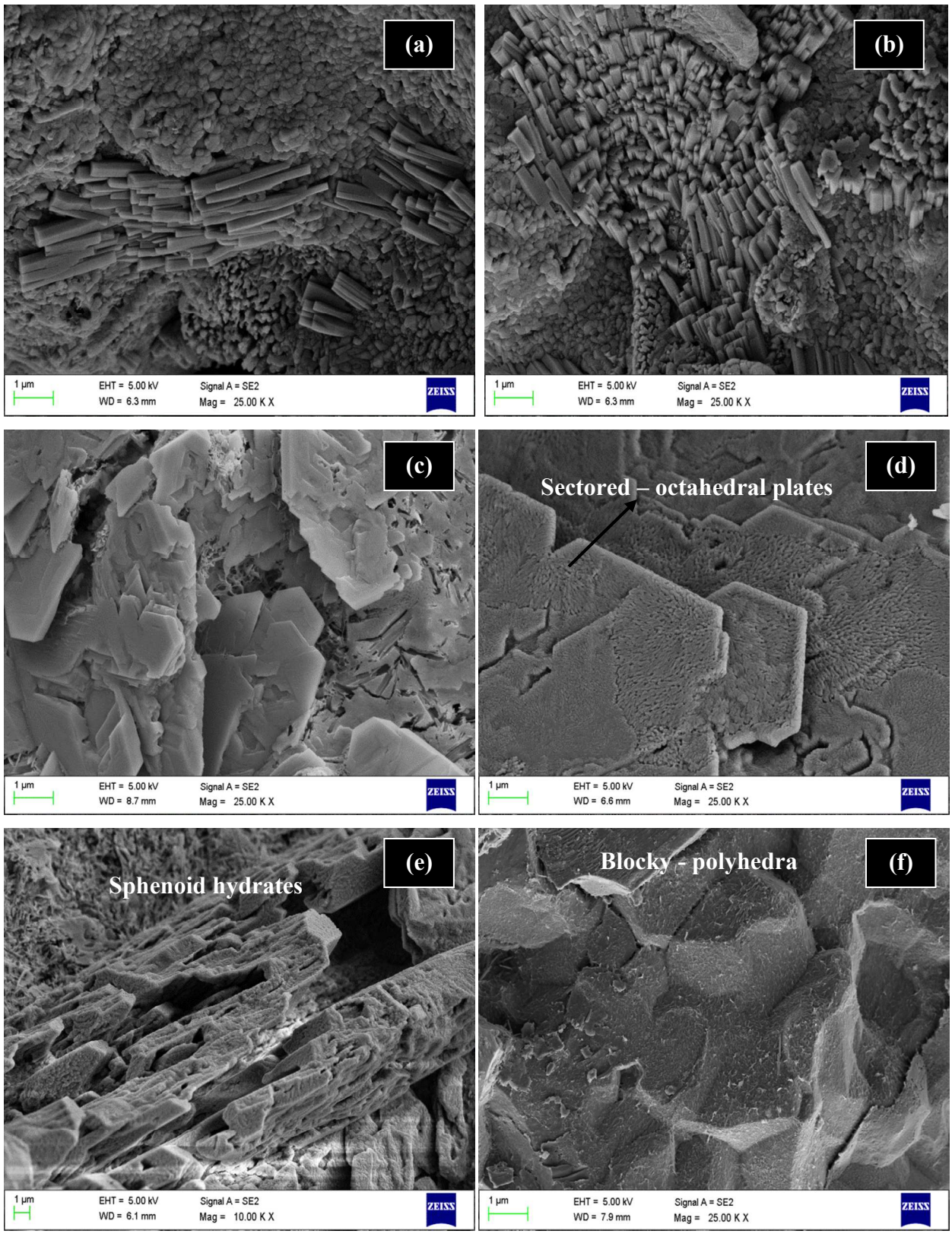

Fig. 12 SEM images of 1.00% (bwoc) GO_a nanocomposites and GO_b nanocomposites after (a & b) 7 days (c & d) 14 days (e & f) 28 days curing respectively

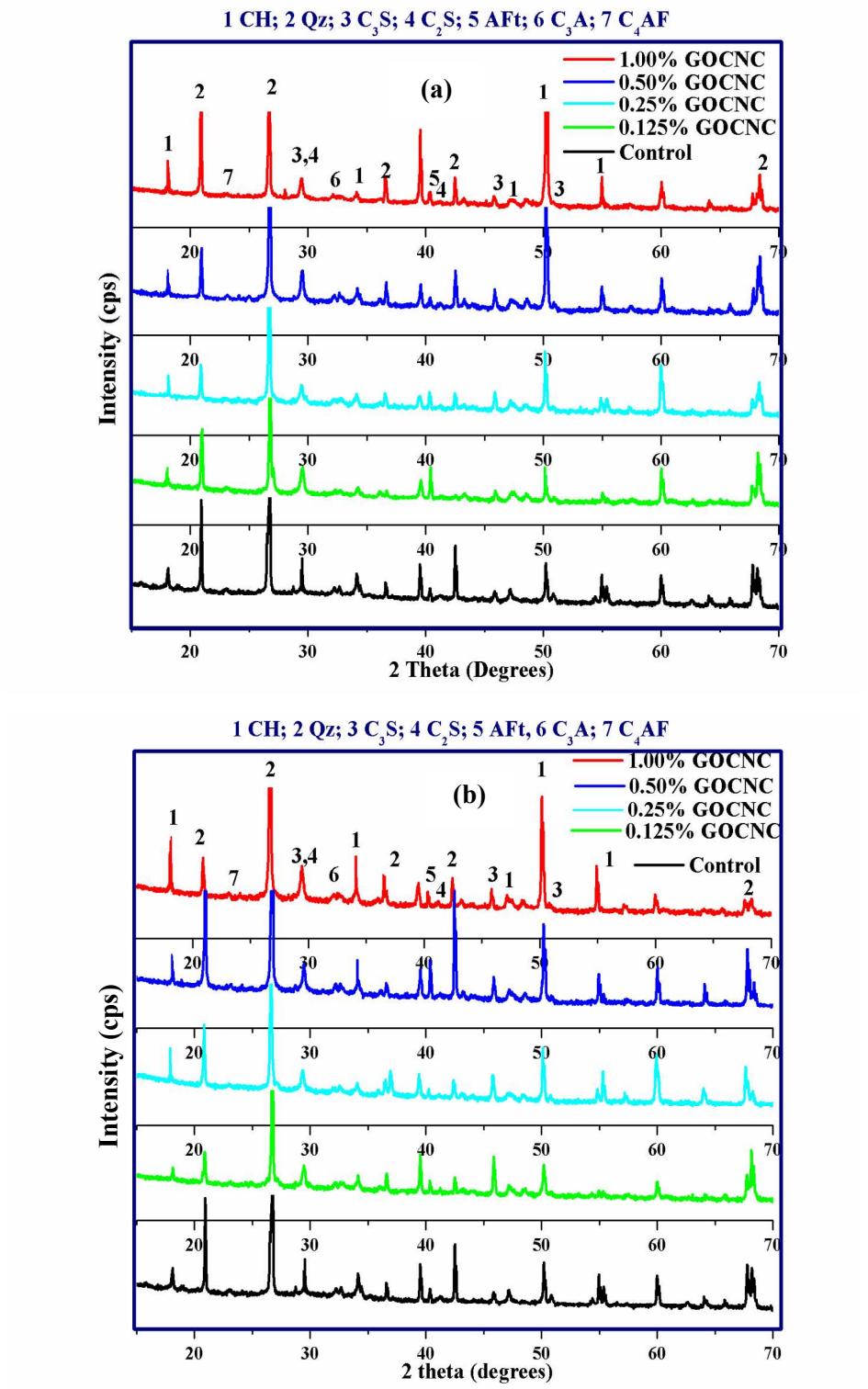

Fig. 13 XRD patterns (a) GO_a - Cement Nanocomposites and (b) GO_b - Cement Nanocomposites (at different GO_a and GO_b concentrations) after 28 days curing

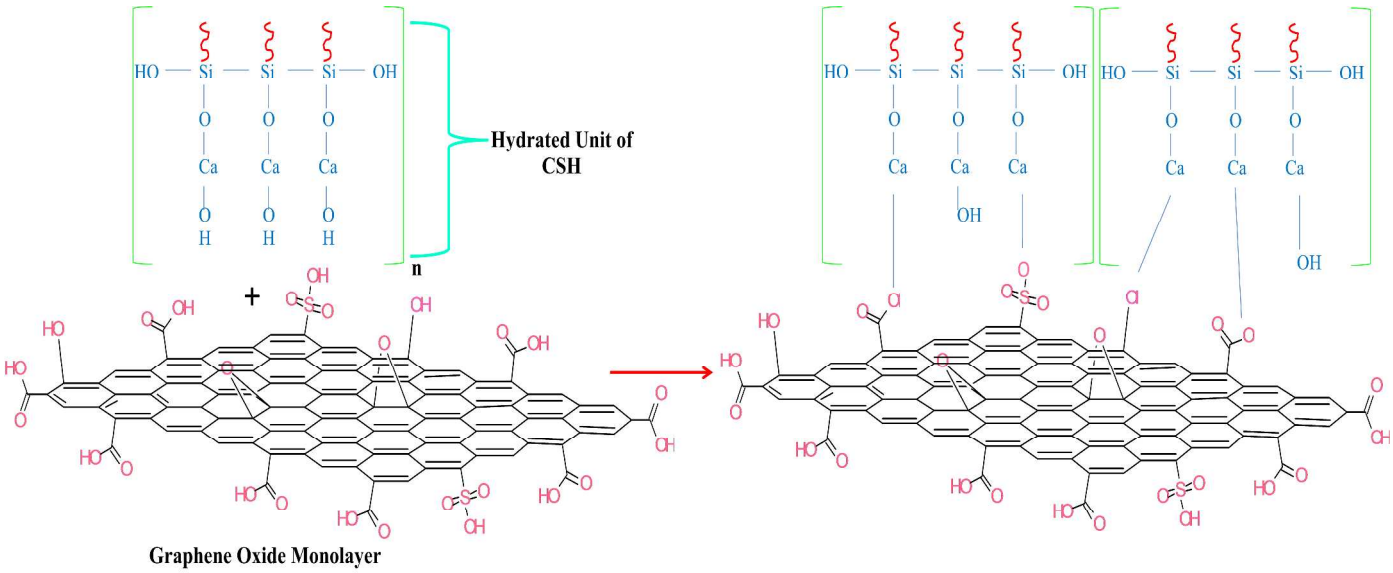

Fig. 14 (a) Schematic showing interfacial bonding between surface functional groups of GO monolayer and hydrated phases of cementitious matrix

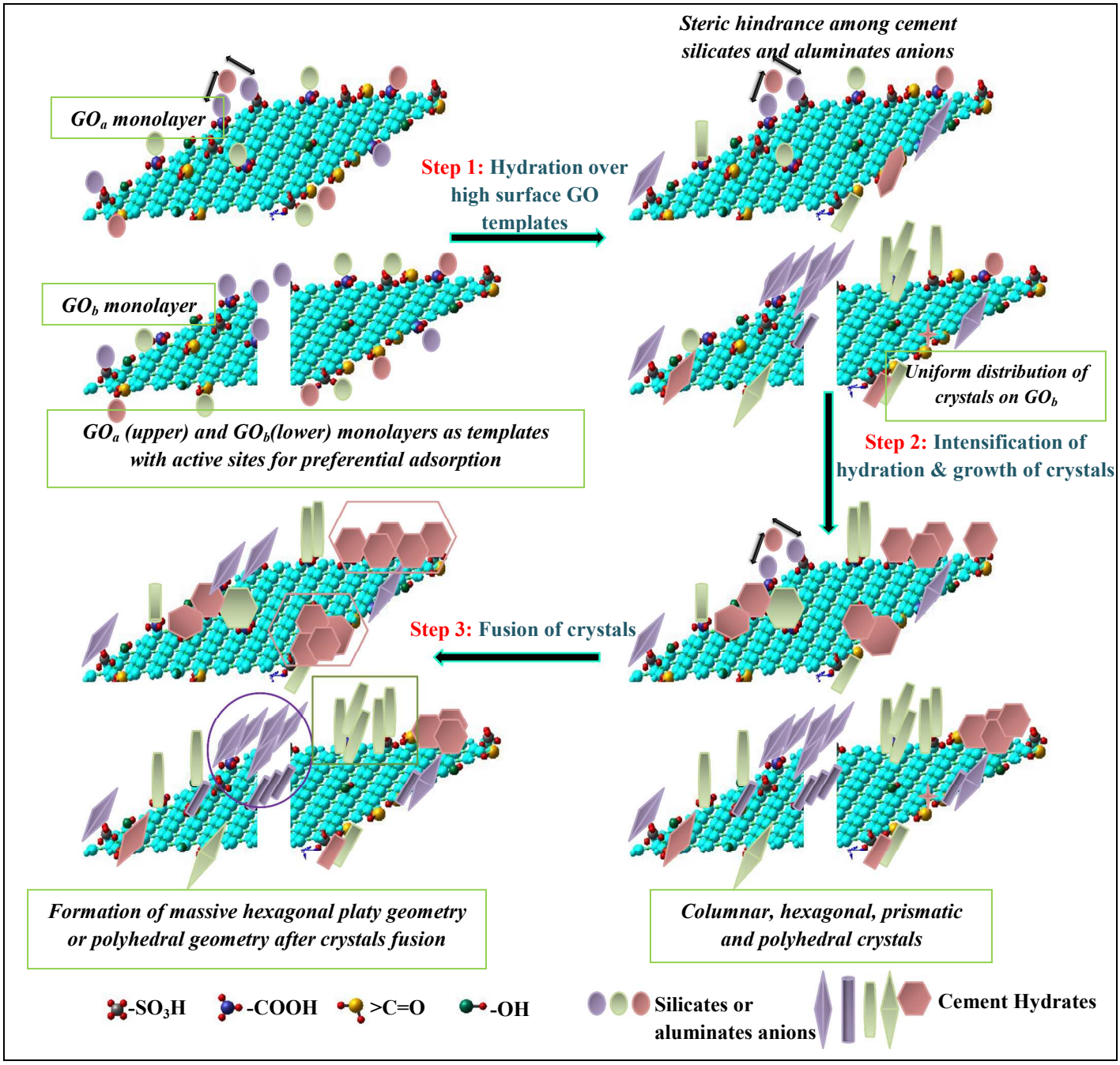

Fig. 14 (b) Schematic showing conversion of growing cement hydrates with definite shapes into fused geometry over GO_a and GO_b templates with active sites